Multi-method absolute paleointensity determinations on a Pliocene multiple-polarity record from the Lesser Caucasus

Elisa M. Sánchez-Moreno[1,*], Manuel Calvo-Rathert[1,7], Avto Goguitchaichvili[2], George T. Vashakidze[3], Pierre Camps[4], Juan Morales-Contreras[2], Néstor Vegas-Tubía[5], Vladimir A. Lebedev[6]

[1]Departamento de Física, EPS Campus Rio Vena – Universidad de Burgos, Av. Cantabria, s/n, 09006 Burgos, Spain.
[2]Laboratorio Interinstitucional de Magnetismo Natural, Instituto de Geofísica Unidad Michoacán, UNAM – Campus Morelia, 58990 Morelia, México.
[3]Alexandre Janelidze Institute of Geology – Ivane Javakhishvili Tbilisi State University, 1/9 M. Alexidze str., 0171 Tbilisi, Georgia.
[4]Géosciences Montpellier, Univ. Montpellier, CNRS, Montpellier, France.
[5]Departamento de Geodinámica, Universidad del País Vasco, E-48940 Leioa, Bizkaia, Spain.
[6]Institute of Geology of Ore Deposits, Petrography, Mineralogy and Geochemistry – Russian Academy of Sciences (IGEM RAS), Staromonetny per., 35, 119017 Moscow, Russia.
[7]Hawaii Institute of Geophysics and Planetology – University of Hawaii at Manoa, 1680 East-West Rd., 96822 Honolulu, HI, United States.

*Corresponding author: emsanchez@ubu.es

Key points

- High reliable paleointensities supported by a multi-method consistency test
- Paleointensity variability in a reverse, intermediate and normal-polarity record
- Successful check of the corrections included in the MSP-DSC protocol

Abstract

We report high technical quality absolute paleointensity determinations from a Pliocene sequence of 20 consecutive lava flows sampled in South Georgia named Apnia, which record either the Gilbert-Gauss polarity reversal or a composite transition from chron C2Ar to subchron C2An-2n. Paleointensity determinations with the multispecimen (MSP) technique were performed on 12 samples with both the original method (MSP-DB) and the extended protocol with corrections (MSP-DSC). Six MSP-DB and eight MSP-DSC determinations passed the proposed quality criteria. MSP-DB yielded higher intensity values than MSP-DSC. In order to provide additional reliability to the results, we have carried out a consistency test by means of a multi-method approach. We have compared the MSP intensities with Thellier-type intensities obtained from the reinterpretation of determinations performed in previous study. The match of both types of paleointensity determinations gives the results an added

reliability. Paleointensity results have been obtained in all 20 flows, 11 of which were supported on different methods. At the reverse polarity lower section, low-VADM values between 2.1 and 4.2 x 10^{22} Am^2 were obtained. The single transitional flow displayed 4.3 x 10^{22} Am^2, and the normal polarity upper section showed higher values between 5.1 and 7.1 x 10^{22} Am^2. The lower section results might be a pre-reversal stage record and the upper section may reflect the intensity recovery after the complete reversal. Furthermore, the results comparison from both methods will allow the evaluation of the quality parameters proposed to MSP method, which are controversial given the novelty of the technique.

Key words: Thellier-Thellier protocol; IZZI protocol; Multispecimen protocols; multi-method paleointensities; high reliable paleointensities; Lesser Caucasus

1. Introduction

Both directional and intensity data are crucial to deeply understand the characteristics of the Earth's Magnetic Field during unstable periods such as reversals or excursions. While paleomagnetic directions can be obtained in a relatively direct way, the absolute paleointensity determination is more complex and time-consuming because the remanent magnetization is proportional, but not equal to the field intensity and there are many processes that can alter the constant of proportionality between both magnitudes. Paleointensity data are less than directional ones because they can only be obtained from materials where the primary magnetization is a thermo-remanent magnetization (TRM), like volcanic rocks. In addition, in paleointensity determinations magneto-chemical alteration of the remanence-carrying minerals should occur during the multiple heating and cooling steps. Furthermore, the laws of reciprocity, independence, and additivity of partial thermoremanent magnetization (pTRM) should be obeyed, which is only the case of the TRM recorded by single domain (SD) and small pseudo-single domain (PSD) grains (Thellier and Thellier, 1959; Dunlop, 2011 and references therein). Multidomain (MD) grains (s.l.) are characterized by different blocking and unblocking temperatures giving rise to so-called pTRM tails (Bol'shakov and Shcherbakova, 1979; Dunlop and Xu, 1994).

This work focuses on the joint analysis of new absolute paleointensity data obtained in the present study with the multispecimen (MSP) method (Biggin and Poidras 2006; Dekkers and Böhnel 2006; Fabian and Leonhardt 2007) and a collection of Thellier-type paleointensity determinations performed previously (Sánchez-Moreno, 2018). This second group of determinations was carried out with the Thellier-Thellier (Thellier and Thellier, 1959) and the IZZI (Yu et al., 2004) methods and results were reinterpreted in this work applying a set of selection criteria commonly used in this type of studies (based on the classical ThellierTool criteria of Leonhardt et al. 2004). Paleointensity determination methods depend on how different energy equilibrium states related to temperature, applied field and demagnetising field are reached

during the experiments. Thus, the use of different methods based on different experimental procedures on samples of the same units, provides an additional strong reliability check with a multi-method consistency test (De Groot et al., 2013; Biggin and Paterson, 2014; Biggin et al., 2015; De Groot et al., 2015; Monster et al., 2015a; Calvo-Rathert et al., 2016; De Groot et al., 2016; Monster et al., 2018), which is one of the aims of the present study.

The MSP-DB is a relatively new paleointensity method supposed to be independent of magnetic domain structure because it presumably eliminates magnetic history effects. The protocol proposes to perform a single heating, trying to minimize the effect of magnetic history due to the presence of MD grains. Fabian and Leonhardt (2010), however, suggest that even so, this method systematically overestimates paleointensity on samples containing MD grains, and thus proposed some additional steps including pTRM normalization, domain-state correction, and an alteration test in a new protocol named multispecimen domain-state-correction (MSP-DSC). Michalk et al., (2010; 2008) and Calvo-Rathert et al., (2016) have also observed paleointensity overestimates with the MSP-DB method on lavas containing a significant MD fraction. Some other studies, however, point to similar values or underestimations with both protocols (Muxworthy and Taylor, 2011; De Groot et al., 2012; Tema et al., 2015, 2016; Calvo-Rathert et al., 2018). Therefore, another aim of the present study is to assess the quality and reliability of the MSP (mainly MSP-DSC) results by comparing them with Thellier-type determinations because the latter are based on a rigorous physical background.

MSP and Thellier-type paleointensity determinations analyzed in the present study have been carried out over the basaltic flow sequence of Apnia (Djavakheti Highland, Southern Georgia), which has been radiometrically dated by Lebedev et al., (2008) yielding K-Ar ages (±2σ) between 3.09 ± 0.10 to 3.75 ± 0.25 Ma. The paleomagnetic directions obtained in this sequence, display either a record of a geomagnetic transition from reversed to normal polarity, likely the Gilbert-Gauss reversal, or a composite transition from chron C2Ar to subchron C2An-2n. Thus, another aim of this work is to analyze the paleointensity variation during such kind of record. From bottom to top of the volcanic sequence, the lava flows yielded 14 reversed, one transitional, and 5 normal paleomagnetic directions. Both mean paleomagnetic poles of the stable polarity populations disagree with the expected pole position for their age but the possible occurrence of tectonic rotations has been ruled out (Sánchez-Moreno et al., 2018).

The paleointensity study on the Apnia sequence has been motivated by previous successful results in other basalt sequences of similar age in the Djavakheti region (South Georgia) (e.g. Borisova & Sologashvili, 1985; Calvo-Rathert et al., 2011, 2013; Camps et al., 1996; Goguitchaichvili et al., 2000, 2001, 2009, 2016). In spite of the excellent characteristics for obtaining paleointensities of this volcanic province; regarding the composition, morphology, formation and arrangement of lava flows, the

number of studies carried out is still scarce in comparison with other locations (e.g. Hawaii, Iceland or Galapagos). In addition, this sequence has a special interest due to the directional data obtained. The record shows normal and reverse polarities separated by a transitional one. Together with this directional record, the paleointensities obtained, provide information about the behavior of the Earth magnetic field during polarity changes. Likewise, the intensity values obtained help us to develop a more rigorous interpretation of the sequence, since the frequency in the flow emission is unknown and we cannot know at what specific moment the polarity reversal/s occurred during the time covered by the formation of such sequence.

As mentioned above, the choice of a multi-method approach is of special interest due to the need to obtain high reliability intensity data. When we analyze the global intensity database, we can see disagreements between data from similar locations and ages and a wide bias in the geographic distribution. Reliable data are necessary to understand how the intensity behaves during and near polarity changes, as well as during stable periods. Regarding the latter topic, the time-averaged value of the Earth's magnetic field strength is the subject of an ongoing intense discussion (e.g. Goguitchaichvili et al., 1999; Heller et al., 2002; Juarez & Tauxe, 2000; Lawrence et al., 2009; McFadden & McElhinny, 1982; Tanaka et al., 1995; Tauxe et al., 2013; Valet et al., 2005; Valet & Fournier, 2016; Wang et al., 2015).

2. Geological setting

The Apnia sequence (41° 21' 40" N, 43° 16' 02" E) was sampled in the volcanic Djavakheti Highland region, located in the central sector of the Lesser Caucasus (South Georgia) (Fig. 1.). This mountain range, which is included in the Alpine-Himalayan belt, is being generated by the still active collision of the Eurasian and Arabian plates. Within the so-called post-collision stage (Adamia et al., 2011) different stages of volcanic activity have taken place (Lebedev et al., 2008) in the Lesser Caucasus area. The volcanism that generates the materials under study corresponds to the 3.7-1.8 Ma phase. A large number of volcanic cones and fissure volcanoes owing to NW-SE and NE-SW extensional strike-slip structures, also developed by the compressional regime (Avagyan et al., 2010), characterize this phase. This volcanism shapes the Djhavakheti and Armenian plateaus and is known as the Akhalkalaki Formation in the Djahavakheti region (Maisuradze and Kuloshvili, 1999).

The Apnia sequence comprises 20 consecutive lava flows of tholeiitic basalts that were sampled from top (AP01) to base (AP20). Between 6 and 12 cores were taken from each successive flow with a portable water-cooled drill and were directly oriented in the field with both a solar and a magnetic compass and an inclinometer. The lowermost dated flow yields a K-Ar age (±2σ) of 3.70 ± 0.20 Ma (flow AP11) and the uppermost one 3.09 ± 0.10 Ma (flow AP01) (Lebedev et al., 2008). In addition, two more dates in flows AP05 and AP08 yield ages of 3.28 ± 0.10 Ma and 3.75 ± 0.25 Ma respectively (Lebedev et al., 2008). The Apnia sequence has been described in a

previous work as a record of a composite transition, either the Gilbert Gauss polarity reversal or a composite transition from chron C2Ar to subchron C2An-2n (Sánchez-Moreno et al., 2018).

3. Rock magnetic and paleomagnetic results

A comprehensive set of rock-magnetic experiments was carried out by Sánchez-Moreno et al. (2018) to determine the carriers of remanent magnetization, to obtain information about their thermal stability, and to estimate the magnetic domain state. These results are used here to select the most promising samples for paleointensity experiments.

Saturation magnetization vs. temperature (Ms-T) curves enabled to distinguish four different kinds of behavior (Fig. S3): i) Type H: Magnetic minerals are characterized by reversible curves with a single Curie temperature (T_C) near to 580°C, corresponding to low-Ti titanomagnetite/magnetite. ii) Type H*: A similar behavior to type-H samples, with the same low-Ti titanomagnetite phase. However, initial and final magnetizations differ by more than ± 15%. In some cases, a weak phase with T_C about 615 °C is detectable. This observation might be attributed to the presence of oxidized magnetite (maghemitization). iii) Type L: This group displays irreversible behavior and two mineral phases. The first phase is observed in the heating curve between 190 °C and 280 °C and matches high-Ti titanomagnetite. The second one is a high T_C phase observed in both heating and cooling curves, which is interpreted again as low-Ti titanomagnetite, and represents only a tiny fraction of the initial magnetization. iv) Type M: It also shows an irreversible behavior and two phases can be distinguished, low-Ti titanomagnetite and an intermediate T_C phase within the 320 °C to 440 °C range in the heating curve.

Hysteresis parameters depicted in a Day plot show that the samples present a PSD-like magnetic behavior, which could also be interpreted as a mixture of single domain (SD) and multidomain (MD). We observe that hysteresis parameters have a certain trend towards MD grains. However, a recent study (Roberts et al., 2018) claims that the Day plots do not lead to a simple and direct inference on the domain states, due to the number of variables that influence the hysteresis curve values.

Thus, magnetic mineralogy experiments indicate a pseudo-single-domain (PSD) titanomagnetite with different titanium contents as the main carrier of magnetization (Sánchez-Moreno et al., 2018).

The analysis of paleomagnetic directions recovered from the Apnia volcanic sequence is consistent with a record of a polarity reversal having taken place between 3 and 4 Ma (Sánchez-Moreno et al., 2018). A succession of 14 lava flows of reversed polarity is shown in the lower part, whose average pole differs from the expected one (Fig. S3). The reversed polarity flows are overlain by a single flow that has recorded a

transitional polarity, with an intermediate VGP latitude of 12.5°. On the top, 5 lava flows display normal polarity, with a mean pole further away from the expected pole than the mean pole of the reverse polarity section. However, the occurrence of tectonic rotations has been ruled out (Sánchez-Moreno et al., 2018). Therefore, a short recording time unable to average PSV and/or an anomalous Earth's magnetic field (EMF) record are both possible interpretations from the directional data of Apnia sequence (Sánchez-Moreno et al., 2018).

4. Polished thin sections analysis

Polished thin sections have been analyzed with reflected light optical microscope and scanning electron microscope (SEM) in order to check the thermoremanent origin of the magnetization, as well as to characterize with more precision, the nature of the mineral carriers of remanence, regarding the textures, morphologies, distribution and sizes of the opaque minerals (i.e. mainly titanomagnetites, see section 3).

Based on the different behaviors of the Ms-T curves, five samples from the Apnia sequence were selected, two from type H and one of each type H*, M and L. The reflected light optical microscopy was carried out in Géosciences Montpellier (Université de Montpellier, France) with a Leitz Orthoplan Microscope. Elaboration of the polished thin sections, backscattered images and composition analyzes were obtained at Universidad del País Vasco (UPV/EHU, Bilbao, Spain). The polished thin sections were carbon coated and analyzed with a JEOL JSM-7000F SEM equipped with an Oxford Inca Pentafet X3 energy dispersive X-ray analyzer (EDX). The EDX microanalyzes were performed with a backscattered electron signal (BSE) at 20 kV and a current intensity of 1×10^{-9} A, with a working distance of 10 mm.

The samples are holocrystalline with micro-porphyric and trachytic textures with vesicles of variable size. They comprise plagioclase, olivine, clinopyroxene, and opaque minerals, as an overall petrological description of the Apnia section. Dominant opaque phases are titanomagnetites and ilmenites with different degrees of oxi-exsolution or intergrowths.

Based on the textures, distribution and sizes of the opaque minerals, two groups of samples can be distinguished: one characterized by the presence of euhedral to subeuhedral crystals with maximum sizes of 140 µm (samples AP02 and AP06; Fig. 1.a and 3.a); and a second one with anhedral opaque minerals with skeletal and dendritic growth morphologies and maximum crystal sizes of 75µm (samples AP08, AP13 and AP14; Fig. 2.d), corresponding to quick quenching sectors of the lava flows. In the former group there are homogeneous, non-exsolved, titanomagnetite crystals as well as titanomagnetites with dense ilmenite intergrowths of Trellis and Sandwich types (Fig. 1.c, d, e and 2.b). According to Haggerty (1991) these intergrowths correspond to textural stages C1 to C3 of high temperature (>600ºC) oxidation of titanomagnetite. Frequently in basalts, ilmenite and magnetite exsolution is likely produced by oxidation

above titanomagnetite T_C during rock formation. This process indicates that original TRM is most likely recorded. Ilmenite crystals also show evidences of oxidation due to the presence of fine ferrian-rutile needles (Fig. 1.c) indicative of an oxidation stage R2 (Haggerty, 1991). Moreover, sample AP06 shows several titanomagnetite crystals undergoing maghemitization along the margins (Fig. 1.b and 2.b), as a product of low-temperature oxidation (<300ºC). This process is related to the high T_C observed in the M_S-T curves. In the latter group, the titanomagnetites show abundant Trellis and Sandwich types of ilmenite intergrowths (Fig. 1.c, d, e and 2.e) categorized as C3 textural stage of oxidation according to Haggerty, (1991). Furthermore, sample AP08 shows small euhedral Ti-poor titanomagnetites in disseminated form (Fig. 1.f and 2.f).

The process of ilmenite intergrowths on titanomagnetites, on the one hand, generates titanomagnetite grains up to 100 times smaller than the original grain, which provides more stable SD grains for the determination of paleointensities. On the other hand, it allows the verification of a high temperature (above Curie temperature) remanence acquisition, suitable for the type of studies that are carried out in this work. The observed maghemitization is an oxidation process at low temperature produced in later stages when the lava is cooling or is already cold. It indicates a probable secondary magnetization that can blur the direction and the intensity determination. Consequently, the samples where maghemitization is observed are discarded for paleointensity experiments.

5. Paleointensity methods

In the present study, paleointensity determinations have been performed with the multispecimen technique without corrections (MSP-DB) (Biggin and Poidras, 2006; Dekkers and Böhnel, 2006) and with corrections (MSP-FC and MSP-DSC) (Fabian and Leonhardt, 2010) at the palaeomagnetic laboratory of UNAM in Morelia (Mexico) and the palaeomagnetic laboratory of Géosciences Montpellier (France). In addition, specific selection criteria (Leonhardt et al., 2004; Paterson et al., 2014) have been applied to intensity values obtained in a previous study (Sánchez-Moreno et al., 2020) on the same flows with the Thellier-Thellier (TT) (Thellier and Thellier, 1959) and IZZI (Yu et al., 2004) methods. Subsequently, theyhave been jointly analyzed with the results from the MSP determinations. The main motivation of this double approach was to provide an additional strong reliability check with a multi-method consistency test. On the other hand, this kind of analysis can also help to evaluate the performance of the MSP method.

5.1. Multispecimen methods

The *multispecimen parallel differential pTRM* method (MSP-DB) (Biggin and Poidras, 2006; Dekkers and Böhnel, 2006) was proposed as a technique fitted to estimating paleointensities independently of domain states of magnetic minerals. Different fields (B_{lab}) are applied to several sister specimens of each sample, parallel to

the original NRM (TRM) and at the same temperature. The temperature is chosen to avoid magneto-chemical transformations, but it must be sufficient to create a TRM spanning an adequate fraction for the paleointensity determination. Therefore, the method provides two advantages over the Thellier type: 1) The magnetic history effects are eliminated if the independence over the domain state structure is assumed. 2) The number of heatings is drastically reduced and the temperature applied is selected to avoid magneto-chemical alterations. Correction steps have been introduced in order to avoid the possible paleointensity overestimation observed in some previous studies (Fabian and Leonhardt, 2007; Michalk et al., 2008, 2010; Calvo-Rathert et al., 2016) on lavas containing a significant MD fraction, questioning the theoretical model first introduced by Biggin and Poidras, (2006). The complete *multispecimen - domain state correction* protocol (MSP-DSC) (Fabian and Leonhardt, 2010) includes the same steps as the original MSP-DB method with three additional heating-cooling cycles. The new steps allow for the correction of the TRM fraction involved in the determination (MSP-FC), reducing the pTRM-tail effect from MD grains (MSP-DSC), and the calculation of the relative alteration produced (see Table S2.).

Measurements were carried out in two different laboratories: *Servicio Arqueomagnético Nacional – Instituto de Geofísica Unidad Michoacaán (IGUM) - Universidad Nacional Autónoma de México (UNAM)* and *Géosciences - Université de Montpellier (France).* The online version Multispecimen Paleointensity 1.5. software (online version http://ambre.gm.univ-montp2.fr/camps/MSP_DSC/) has been used for the interpretation of MSP results.

The sample pre-selection criteria in the UNAM laboratory were the following: a univectorial ChRM component, the presence of reversible Ms-T curves (H and H* types), a median destructive field (MDF) > 25 μT in alternating field (AF) demagnetizations and magnetization drops at high temperatures in the thermal demagnetization experiments. The chosen temperature was 450°C, at which 75% of the magnetization still remains. B_{lab} was applied at intervals of 5 or 10 μT, according to the results being obtained, within a range of 5/10 μT to 80 μT, on 7 specimens from each studied lava flow for the MSP-DB protocol and on 4 to 5 specimens for the MSP-DSC protocol. Small irregular fragments were taken from standard samples and prepared in $10cm^3$-standard size salt pellets. The salt samples were placed in a mu-metal home-made sample holder, heated with the TD48-DC (ASC) thermal demagnetizer, and measured with a JR-6 spinner magnetometer (AGICO).

In Géosciences – Montpellier, the samples were chosen under the same pre-selection criteria as in UNAM. In addition, the specimens of the same core had to show Arai plots without negative pTRM checks in previously performed Thellier-type experiments (Sánchez-Moreno et al., 2020). The heating temperature was also set at 450°C. At this temperature the selected samples still retain between 20% and 80% of the TRM in the Thellier-type experiments and it is low enough to avoid magneto-chemical alteration. B_{lab} was applied in intervals of 10 μT, from 10 μT to 80 μT, to 8

specimens from each selected lava flow. Small irregular fragments were taken from standard samples and were prepared in 10-cm^3-standard size plaster. The samples were heated in the FURéMAG prototype furnace (Patent # 1256194). A precise magnetic induction field, perfectly controlled in 3D with a precision better than 1°, was applied to each sample during heating and/or cooling. Fanjat (2012) showed that it is not necessary to apply a cooling rate correction with the MSP protocol (Tema et al., 2015) during the test and the calibration of this furnace. Measurements were performed with a superconducting magnetometer (2G Enterprise).

When the sample's individual declination and inclination measured at different steps was found different to the original NRM, they were not corrected, as it is impossible to apply a correction to the angle due to pTRM-tails caused by MD grains. However, when the maximum angle between the NRM after pTRM acquisition and the total NRM exceeded a critical angle of 10°, the measurement for that specimen was dismissed. Parameter α (Fabian and Leonhardt, 2010) is a constant to calculate the contribution of the domain state effect, used to avoid a possible overestimate of the domain-state contribution. In this work an α = 0.5 value is taken for the calculations. A set of criteria based on the linear regression analysis and correction ratio Q_{DB}, Q_{FC} and Q_{DSC} calculations (Fabian and Leonhardt, 2010) under MSP-DB, MSP-FC and MSP-DSC protocols, was used to select the individual MSP data and reject those of poor technical quality (Table S3).

5.2. Multispecimen results

Seven MSP determinations on single cores belonging to 7 different lava flows were measured in the UNAM laboratory and 5 MSP determinations were carried out on samples from 5 different lava flows in Géosciences – Montpellier. In this latter case, the specimens for each determination were taken from a single core in 3 cases, and from different but nearby cores in 2 cases (cores 03 and 04 separated 40 cm in AP01 and cores 07 and 09 separated 2 m in AP20). In all, MSP paleointensity determinations could be performed on 12 of the 20 flows comprising the Apnia sequence. Table S1 shows the quality criteria used to select successful paleointensity determinations. Two sets of threshold values of different stringency were chosen to distinguish between two different determination quality levels, class A and class B (Table S3). After applying the proposed threshold criteria, 6 MSP-DB determinations from a total of 12 are considered as reliable (Table 1), all of them belonging to class B. The determination obtained for flow AP03, however, shows a high relative error ΔB (ΔH from Fabian and Leonhardt, (2010), Table S1). Because AP03 meets all remaining criteria, it has been labeled as class B*. It should be mentioned that error parameters ε_{alt} (and also ΔB) may, in theory, also be applied to MSP-DB. Although they cannot be calculated for the MSP-DB protocol, the same processes that generates these errors in the MSP-DSC experiments, also occur in MSP-DB because the temperature attained is the same.

Eight successful determinations were obtained with the MSP-DSC protocol, (67% success rate) 2 of them belonging to class A, five to class B and sample AP03 again to B*(Fig. 3 and Table 3). Paleointensities obtained under the MSP-DB protocol range between 14 and 67 µT, while MSP-DSC paleointensities yield values between 14 and 55 µT, except for AP05, which despite passing all quality criteria, yields an apparently more anomalous value of 100 µT (Table 1).

Another interesting result arising from the comparison of the *multispecimen parallel differential pTRM method* (MSP-DB) (Biggin and Poidras, 2006; Dekkers and Böhnel, 2006), *multispecimen - fraction correction* (MSP-FC) and *multispecimen - domain state correction* (MSP-DSC) (Fabian and Leonhardt, 2010) protocols, is their relationship in terms of the paleointensity value. In previous works, an overestimation of DB over DSC paleointensities of up to 20% was observed (Fabian and Leonhardt, 2007; Michalk et al., 2008, 2010; Calvo-Rathert et al., 2016). In this work, DSC paleointensities weaker than DB ones have been obtained in all determinations, except in AP20, where intensities FC>DSC>DB. In AP14 DB, FC and DSC values are indistinguishable.

5.3. Thellier-type determinations

In a previous study (Sánchez-Moreno et al., 2020), Thellier-type paleointensity determinations with the original Thellier-Thellier (TT) protocol (Thellier and Thellier, 1959) and the IZZI protocol (Yu et al., 2004) have been performed on samples from all 20 flows of the Apnia sequence. TT experiments were carried out in the paleomagnetic laboratory of the University of Burgos on small cylindrical specimens of 8 mm diameter with a TD48-SC (ASC) thermal demagnetizer under argon atmosphere. IZZI experiments were carried out in the paleomagnetic laboratory of the Scripps Institution of Oceanography, UCSD (USA) with specimens prepared as small irregular fragments in 10 mm diameter vials. Experiments were performed in a homemade single chamber thermal demagnetizer under air. In both cases, laboratory field B_{lab} was set at 40 µT and several pTRM checks were performed.

The Thellier GUI PmagPy package software (Tauxe et al., 2016) was used for the interpretation of results obtained with both protocols. A set of especially strict selection criteria (Tauxe et al., 2016) was used to assess the quality of the experiment conditions, the absence of alterations and the amount of magnetization carried by multidomain grains (MD). Application of this very strict set of criteria yielded 4 out of 55 reliable absolute paleointensity determinations with the TT method and 41 out of 100 with the IZZI method, yielding paleointensity results in 8 of 20 studied lava flows at the site level. At the reverse polarity lower Apnia section, low VADM values between 2.9 and 4.6 × 10^{22} Am^2 were obtained, while the normal polarity upper section displayed a single value of 5.6 × 10^{22} Am^2. All these paleointensity values lie well below the present-day dipole moment in Georgia (8.4 × 10^{22} Am^2).

One of the aims of the present study was to provide an additional reliability check with a multi-method consistency test. A positive consistency test would ensure the reliability of determinations retrieved from Thellier-type and MSP determinations with matching paleointensity values (e. g. Monster et al., 2015a; Calvo-Rathert et al., 2016; De Groot et al., 2016)., as a match obtained from two failed experiments performed with different methods would be highly unlikely. In fact, Biggin and Paterson, (2014) suggest that the average per site must include paleointensities from more than one technique. A first condition to perform a comparison between Thellier-type and MSP results is that both have been obtained from successful determinations. As mentioned above, selection criteria applied by Sánchez-Moreno et al. (2020) were especially strict. However, when the multi-method consistency test is applied, it would be not necessary that parameters of selection criteria for the Thellier-type experiments are so strict. On one hand, although it is still necessary that the final results are able to stand by themselves, the multi-method consistency check can provide an additional confirmation of the results. In addition, as noted by Patterson et al. (2014), some set of criteria can be too strict, as they lead to the rejection of ideal samples subject to experimental noise. For this reason, we have performed a new interpretation of our experimental Thellier-type determinations (Table S4 and S5), not using the criteria of Tauxe et al.(2016), but the still reliable and commonly used ThellierTool criteria (Leonhardt et al., 2004) as modified by Paterson et al. (2014), allowing two quality levels A and B (Table S2), in order to perform a multimethod consistency check together with the results obtained with the MSP determinations from the present study.

6. Discussion

One of the aims of the present work is to analyze the paleointensity variation along a lava flow sequence including a polarity transition. For this analysis, reliable paleointensity data, ideally for each lava flow are needed. The comparison of the results obtained from the different types of paleointensity determination experiments may reinforce their reliability. Two different Thellier-type methods (Thellier-Thellier and IZZI) and the MSP method including three different protocols including corrections have been considered. There is a general agreement among the paleomagnetic community that Thellier-type methods should be considered as the most reliable ones because of their robust physical basis. MSP methods, however, are more recent and still need to be substantiated, for which a greater number of data is needed. To accomplish these goals, the rationale of the multi-method approach used in the present study has been the following:

(i) Results of both Thellier-type and multispecimen determinations are obtained after applying specific selection criteria to select reliable paleointensity determinations.

(ii) Successful Thellier-type paleointensity determinations are used to evaluate the quality of multispecimen determinations, as Thellier-type methods are considered the most reliable.

(iii) Agreement of paleointensity results from multispecimen and Thellier-type determinations is considered as an added strong indicator of a successful paleointensity determination, as a match obtained from two failed experiments performed with different methods can be considered highly unlikely.

MSP results and some criteria used to select them will be discussed in the following sections.

6.1. MSP method and quality criteria

The fraction range f (Fabian and Leonhardt, 2010) is the ratio between the fraction of NRM removed and overprinted by the laboratory pTRM for each point, i. e. for each specimen subjected to a different B_{lab}. The commonly proposed threshold values lie between 0.2 and 0.8 (20% and 80% of the total NRM). In this interval, the fraction is large enough to be accurately measured and still clearly below a total TRM (Tema et al., 2016). It is obtained from the half vector sum between measurements m1 and m2 of the MSP-DSC procedure (Table S2) normalized by the NRM, and for this reason it can only be calculated for the FC and DSC determinations. Even so, we consider that it is also applicable to the original DB method, because it depends on the temperature reached during the experiment (and therefore on the amount of TRM unblocked and overprinted), which in the three MSP variants is the same. In the present study, it was decided to apply 450°C to all samples, but in some determinations, f is less than 0.2. In such cases, a higher temperature would have been more adequate, since the magnetization drop in these samples occurs at slightly higher temperatures, and the f-range used in the MSP experiments is sensitive to the temperature applied. Comparison with Thellier-type experiments, however, shows that some determinations in which f < 0.2 (AP11, AP15 and AP19) yield similar paleointensities (see section 7.2.). This observation may indicate that a lower f range may be valid in MSP in some specific cases. In the present study, these three determinations have not been formally considered reliable MSP determinations in Table 1, but their agreement with Thellier-type results (see discussion below) has driven us to consider them for final paleointensity calculations. In Table 1 they have been named as Thellier-validated (T^V) results.

The average alteration error ε_{alt} (Fabian and Leonhardt, 2010) is also one of the new quality criteria used in the MSP-DSC protocol. It is calculated with measurement m1 and repeated measurement m4 of the of the MSP-DSC procedure (Table S2). As it is considered that for thermo-chemical changes the temperature attained is more important than the number of heatings, it is possible to use ε_{alt} for all MSP variants. Monster et al., (2015a and b) have proposed a strict threshold of 3%, which is used by Calvo-Rathert et al., (2016), while Tema et al., (2016) take a more flexible 10%. Comparing the obtained MSP paleointensity values with the Thellier-type ones (as will be discussed in the next section) and analyzing their coincidences, in this work 10% is used for class A and 15% for class B determinations.

Parameters ΔB (ΔH from Fabian and Leonhardt, 2010) and CI_{95} (see Multispecimen Paleointensity 1.5. software online version http://ambre.gm.univ-montp2.fr) provide an estimation of the uncertainty. CI_{95} is the bootstrapped 95% confidence interval calculated and critically evaluated with the Shapiro-Wilk test of normality (see MultiSpecimen Paleointensity software online version http://ambre.gm.univ-montp2.fr/camps/MSP_DSC/). It is in reasonably good agreement and within the error bar compared to the value obtained with the conventional Thellier protocol (Tema et al., 2015). An almost ideal determination is achieved when the upper and lower limits are symmetrical with respect to the paleointensity value. ΔB is the final error of the determination obtained by the total error of each specimen used in the determination (see ΔQ_i in Table S3). To find out ΔB, the alteration-induced error (which includes ε_{alt}) and the approximation of the absolute error of the domain-state correction are calculated. Like the relative alteration error ε_{alt}, ΔB also depends on the temperature reached, and hence it may be considered to evaluate the quality of DB and FC determinations as well as those of the DSC. In the present study, the results provided in several cases by CI_{95} and ΔB are contradictory. In such cases, only the CI_{95} parameter is taken into account.

6.2. MSP vs. Thellier-type

In this section, the agreement between mean flow paleointensities obtained with Thellier-type and MSP methods will be analyzed. For this comparison, and later calculation of the final flow-average paleointensities (Table 3), the results obtained with the DSC protocol have been considered as more reliable (see section 6.3) than those obtained with the MSP-DB protocol. It must be noted that some MSP-DSC paleointensities do not pass all quality criteria but agree with those obtained with Thellier-type methods

All flows have been grouped according to the agreement of their MSP-DSC and Thellier-type paleointensity results together with their technical quality. For this classification, we assume that TT-IZZI and MSP-DSC mean paleointensities agree if the difference between them is less than 8 μT. The use of relative differences to quantify the agreement of results in the lower section implies too small errors when compared to the experimental results. Consequently, a standard value has been chosen. In this case, it is 15% of the present-day field in Georgia (50 μT), which is approximately 8 μT. The problem of applying the same percentage to both low and high paleointensities is discussed in Tauxe and Staudigel, (2004) and Tauxe, (2006). The following types of behavior can be distinguished:

Class 1. Good technical quality MSP-DSC paleointensities agree with Thellier-type ones: This case is observed for flows AP01, AP14 and AP17.

Class 2. Good technical quality MSP-DSC paleointensities disagree with Thellier-type ones: This case happens in flows AP03, AP04, AP05, AP10 and AP12. Here, MSP-DSC determinations are rejected because the reliability of Thellier-type methods over MSP is *a priori* assumed. In addition, the Thellier-type determinations are based on a greater number of determinations.

Class 3. Bad quality MSP-DSC paleointensities agree with Thellier-type ones: This case could be observed in flows AP11, AP15, AP19 and AP20. In such case MSP-DSC data support the reliability of Thellier-type results. This case may raise doubts about the chosen threshold values from the quality parameters used (see section 7). Only AP11 and AP19 do not fit the quality criterion f. As discussed in the previous section, we consider them reliable with $f < 0.2$.

The comparison of results obtained from MSP and Thellier methods can also supply interesting information regarding the supposed ability of the first one to provide successful results. Especially in those cases when TT or IZZI display concave-up-shape Arai plots which are not able to deliver reliable paleointensity results. For flow AP01, specimens from two different samples (03A and 04A) have been used in an MSP-DSC determination, which pass the quality criteria. In a specimen of the same sample 03A, an IZZI determination with a concave-up shape Arai plot was detected. Specimen 04A, on the other hand, shows a linear-shape Arai plot, but a MD trend in the Day-plot. In flow AP05, sample 01B displays a concave-up-shaped Arai plot and a successful MSP-DSC determination. Therefore, we believe that the MSP-DSC determination behaved independently of the domain state in these samples.

Biggin and Paterson, (2014) suggest that a site-average must include paleointensities from more than one technique to support results of high reliability. In addition, they propose a new set of largely qualitative reliability criteria for paleointensity results at the site mean level, which they term Q_{PI}. They intend to identify biasing agents applicable to paleointensity measurements which are sometimes obviated to quantify the reliability of the paleointensity values obtained from a study. The Q_{PI} criteria and the fit of our results to them are the following:

1. AGE: Apnia paleointensity results show a reliable age and paleomagnetic behavior derived from a primary component of remanence.
2. STAT: 10 lava flows passed the requirement of 5 individual specimens used in the average paleointensity (AP01, 02, 04, 11, 14, 16, 17, 18, 20 and 19). It is worth mentioning that 5 flows have 3 or 4 specimens in the average (AP05, 06, 07, 09, and 13), as commonly, 3 paleointensity determinations are considered a good average.
3. TRM: Microscope analysis supports the evidence that the remanence is a thermoremanence.
4. ALT: pTRM checks and rock mag experiments (also ε_{alt} parameter in MSP) support that there is not alteration.

5. MD: A high f parameter in Thellier-type and domain state correction in MSP-DSC determinations verify that the MD effect does not affect the final paleointensity estimate.
6. ACN (Anisotropy of TRM, Cooling rate and Non-linear TRM effects):
   - Anisotropy of TRM: Anisotropy of magnetic susceptibility (AMS) was measured on one sample from each flow showing a corrected anisotropy P' value (Jelinek, 1981) of approximately 4% (P' between 1 and 1.040, average 1.014, Sánchez-Moreno et al., 2020?). The gamma statistic γ (Paterson et al., 2014) in both the Thellier-Thellier and IZZI determinations yields values between 0.2° and 3.7°. Only when gamma >> 4° it is considered that there is a higher chance that the specimen is anisotropic (Paterson et al., 2015).
   - Cooling rate: The lava flows characteristics (thickness, composition, etc.) allow the assumption that the cooling-rate does not affect the paleointensity experiments, given that it does not vary significantly in the range of thickness of the individual cooling units. The Thellier-Thellier and IZZI experiments have been performed by cooling the samples under natural conditions (~10h) and with a fan (~1h) respectively (Sánchez-Moreno et al., 2020), without differences in the results.
   - Non-linear TRM effects: They are minimal when the laboratory and ancient field strengths are approximately equal (Paterson, 2013; Selkin et al., 2007). For most typical geological materials (i. e., lavas), if both fields are within ~1.5 times each other, the influence of non-linear TRM is likely to be minimal (Biggin and Paterson, 2014).
7. TECH: Final paleointensity from 11 lava flows have been calculated from more than one technique (AP01, 02, 04, 07, 11, 13, 14, 17, 18, 20 and 19).
8. LITH: The paleointensity estimations have been performed over samples of similar lithology and with similar unblocking behavior.

From this analysis 10 final mean paleointensities (lava flows AP01, 02, 04, 11, 14, 16, 17, 18, 20 and 19) can be classified as Q_{PI} = 7. AP07 and AP13 show a Q_{PI} = 6. Lastly, the 8 remaining final mean paleointensities have Q_{PI} = 5.

6.3. Paleointensity average per lava flow

As mentioned above, three different types of paleointensity determinations have been used and results show a rather large variability. Now, the question of how to calculate an average intensity per lava flow that is reliable and representative is raised. It should be considered that the paleointensity for each lava flow has been averaged for each method if determinations passed the proposed quality thresholds. In addition, for MSP-DSC determinations, the agreement with Thellier-type results is considered as decisive. In doubtful cases, the agreement with paleointensities obtained in adjoining flows is also taken into account. Mean paleointensities have been weighted according to the number of determinations of each method (Table 3), and the valid average paleointensity per flow must have a standard deviation value

within ±25%. According to the methods involved in the average, various quality levels can be distinguished.

Quality 1: Average paleointensity per lava flow calculated with at least one Thellier-type determination and one MSP-DSC determination of good quality and matching Thellier results. Flows AP01, AP14 and AP17 present the most reliable paleointensities (Table 3) yielding quality 1 results.

Quality 2: Three or more TT and IZZI determinations comprise the average. Alternatively, at least a single Thellier-type determination and an MSP-DSC determination that do not reach all quality thresholds but match the results obtained with the Thellier method (AP11, AP15, AP19 and AP20). In this latter case, the average paleointensity has been calculated without MSP-DSC (Table 3). In total, nine Quality 2 determinations have been obtained.

Quality 3: Three or more determinations of a single Thellier-type method. Alternatively, a reliable MSP determination together with a Thellier-type experiment yielding a concave up Arai plot. However, no reliable MSP determinations accompanied by a concave up Arai plot were obtained in all the sequence. MSP-DSC results from AP05 yielded acceptable quality parameters, but the paleointensity value obtained displays an abnormally strong value, which clearly disagrees with the Thellier-type results. Therefore, this value has been discarded and only the average obtained from 4 IZZI determinations has been selected in AP05.

Quality 4: Less than three determinations of a single Thellier-type method. They are taken into account if they match the adjacent lava flow paleointensities, as is the case of AP03, AP08, AP10 and AP12. Flow AP03 might present the most questionable result because it has been obtained from a single Thellier-Thellier determination. Nevertheless, it agrees with the results from the adjacent flows.

Finally, average paleointensities have been obtained for all the 20 flows that comprise the Apnia sequence (Table 3 and Fig. 3). Three paleointensities belong to quality level 1, nine to quality 2, four to quality 3 and four to quality 4. Paleointensity values in the lower section of reverse polarity range between 12.5 μT and 24.6 μT. The intermediate polarity flow gives a value of 25.2 μT. In the upper section of normal polarity, the paleointensities show higher values, which range between 29.9 μT and 41.5 μT. The virtual axial dipole moment (VADM) has also been calculated for the final average paleointensities (Table 2, yielding values of between 2.1 and 4.1 × 10^{22} Am^2 in the reverse polarity part, 4.3 × 10^{22} Am^2 in the transitional polarity flow and in the normal polarity section between 5.1 and 7.1 × 10^{22} Am^2.

6.4. Directional results vs. paleointensities

Paleomagnetic directions obtained in Apnia lava sequence are consistent with a record of a polarity reversal (Sánchez-Moreno et al., 2018). According to radiometric ages (Lebedev et al., 2008), the record may correspond either to the Gilbert-Gauss reversal (C2Ar to C2An-3n) or to a composite transition record from C2Ar to C2An-2n subchrons (Fig. S3). Moreover, Sánchez-Moreno et al. (2018) concluded that the analysis of paleomagnetic directions in combination with the virtual geomagnetic pole scatter and a few previously available paleointensity results (Calvo-Rathert et al., 2013), enable two non-exclusive interpretations: an anomalous EMF record or a short recording time unable to average paleosecular variation. As mentioned above, the flow-average paleointensities obtained in the present study range from 12.5 to 24.6 μT in the lower reverse-polarity section, the transitional flow yields 25.2 μT and the upper normal-polarity section provide higher values between 29.9 and 41.5 μT. All obtained intensity values are below the present field strength in Georgia (about 50 μT). During large departures of the geomagnetic field from the GAD, the intensity decreases significantly (e.g., Laj and Channell, 2007 and references therein). Furthermore, the intensity variation begins before the direction variation (Prévot et al., 1985a; Prévot et al., 1985b; Herrero-Bervera and Valet, 1999; Riisager et al., 2000). Under these circumstances, it is possible to interpret that the lower part of the Apnia sequence records the initial stage of the reversal, whereas the upper section shows the recovery of the EMF intensity, after the polarity transition.

The multi-method approach applied in the present study provides consistent paleointensity results in all flows of the sequence, allowing to support the previous directional interpretation of the record as a polarity reversal. It is, however, an arduous methodology which involves carrying at least two types of experiments. In comparison with other approaches to obtain high quality paleointensities, such as applying very strict selection criteria to Thellier-type determinations (Tauxe et al., 2016) which is less laborious, a higher number of reliable data might be obtained from the same data population (Sanchez-Moreno et al., 2020).

7. Conclusions

An inter-laboratory and multi-method absolute paleointensity determination study has been carried out on the Pliocene Apnia sequence that is composed of 20 consecutive lava flows. According to paleomagnetic directions and available radiometric ages, the sequence seems to record either the Gilbert-Gauss reversal or a composite polarity transition from chron C2Ar to subchron C2An-2n (Sánchez-Moreno et al., 2018). Moreover, paleomagnetic results of the reverse polarity section provide two different but not conflicting interpretations: a relatively short recording time unable to average PSV and/or an anomalous EMF record (Sánchez-Moreno et al., 2018).

Absolute intensity determinations with the multispecimen technique were performed on 12 samples with both the original method (MSP-DB, Biggin and Poidras, 2006; Dekkers and Böhnel, 2006) and the extended protocol with corrections (fraction correction FC and domain state correction DSC; Fabian and Leonhardt, 2010). Eight MSP-DSC determinations from eight flows passed the proposed quality criteria.

In a previous study (Sánchez-Moreno et al., 2020), Thellier-type paleointensity determinations with the original Thellier-Thellier (TT) (Thellier and Thellier, 1959) and the IZZI protocol (Yu et al., 2004) had been performed on samples from all 20 flows of the Apnia sequence, yielding paleointensity results in 8 of 20 studied lava flows. One of the aims of the present study was to provide an additional reliability check with a multi-method consistency test including results from both Thellier-type and MSP determinations. For this reason, we have performed a new interpretation of these experimental Thellier-type determinations with the commonly used ThellierTool criteria (Leonhardt et al., 2004) as modified by Patterson et al. (2014), in order to perform a multimethod consistency check together with the results obtained with the MSP determinations from the present study.

Paleointensity results could be obtained in all 20 lava flows, and 11 flow averages are supported on different methods. The flow-average paleointensities obtained this way range from 12.5 to 24.6 μT in the lower reverse-polarity section, the transitional flow yields 25.2 μT and the upper normal-polarity section provide higher values between 29.9 and 41.5 μT. All obtained intensity values lie below the present field strength in Georgia (about 50 μT). The reverse polarity lower part yielded relatively low-paleointensity values, characteristic of pre-reversal stages (Laj and Channell, 2007). The relatively high paleointensity values recorded in the upper part of normal polarity may reflect the intensity recovery after a complete reversal.

Comparison of MSP-DB and MSP-DSC results with known field values for the same location and age shows a paleointensity overestimation by the method without corrections, also reported in some previous studies (Michalk et al., 2008a, 2010; Fabian and Leonhardt, 2010; Calvo-Rathert et al., 2016), in contrast to other works where the results from both protocols are similar or the MSP-DB protocol underestimates the paleointensity values (Muxworthy and Taylor, 2011; De Groot et al., 2012; Tema et al., 2015, 2016; Calvo-Rathert et al., 2018). Therefore, according our results, the MSP-DB method is not independent of domain structure. Moreover, the introduced correction steps with the MSP-DSC protocol prevent paleointensity overestimation, and thus it is recommended to use the MSP-DSC protocol instead of the original MSP-DB one.

Yet, no generalized agreement may be reached about the quality criteria used in MSP paleointensity determinations and their threshold values. In the present study we prefer to use CI_{95} (95% confidence interval, see Multispecimen Paleointensity 1.5. software online version http://ambre.gm.univ-montp2.fr/camps/MSP_DSC) over ΔB (ΔH in Fabian and Leonhardt, (2010) as a measure for the final uncertainty of the

determination. It should be noted, however that CI_{95} is calculated through bootstrapping and is only valid if the bootstrapped values have a Gaussian distribution. We also propose a less strict threshold (10-15%, depending on determination quality level) for the relative alteration error ε_{alt}, than previously recommended by Monster et al. (2015a and b). In some determinations, in which MSP-DSC paleointensities were close to those obtained with Thellier-type methods, the f-factor was below the required 0.2 threshold. This evidences that reliability criteria still need to be analyzed in detail.

Acknowledgements

This work was supported by project CGL2012-32149 (MINECO, Spain), project BU066U16 (Junta de Castilla y León, Spain) and pre-doctoral grant BES-2013-064060 (MINECO, Spain). MCR acknowledges funding from the Fulbright Commission and the Spanish Ministry of Science, Innovation and Universities for a research stay at Hawaii University at Manoa. AG is grateful to the financial support given by DGAPA-PAPIIT IN101717. At Montpellier laboratory, the FUReMAG rapid furnace construction was supported by the French National Agency for Research (ANR-12-BS06-0015). Datasets for this research are available in these in-text data citation references: Sánchez-Moreno, E. M. (2020). Thellier and multispecimen paleointensities from Apnia Pliocene volcanic sequence [Data set]. Zenodo. http://doi.org/10.5281/zenodo.3673186

References

Adamia, S., Zakariadze, G., Chkhotua, T., Sadradze, N., Tsereteli, N., Chabukiani, A., Gventsadze, A., 2011. Geology of the Caucasus: A Review. Turkish J. Earth Sci. J. Earth Sci.) Copyr. ©TÜBİTAK 20, 489–544. https://doi.org/10.3906/yer-1005-11

Avagyan, A., Sosson, M., Karakhanian, A., Philip, H., Rebai, S., Rolland, Y., Melkonyan, R., Davtyan, V., 2010. Recent tectonic stress evolution in the Lesser Caucasus and adjacent regions. Geol. Soc. London, Spec. Publ. 340, 393–408. https://doi.org/10.1144/sp340.17

Besse, J., and V. Courtillot (2002). Apparent and true polar wander and the geometry of the geomagnetic field over the last 200 Myr, J. Geophys. Res., 107(B11), 2300, doi:10.1029/2000JB000050.

Biggin, A.J., Paterson, G. a., 2014. A new set of qualitative reliability criteria to aid inferences on palaeomagnetic dipole moment variations through geological time. Front. Earth Sci. 2, 1–9. https://doi.org/10.3389/feart.2014.00024

Biggin, A.J., Perrin, M., and Shaw, J., 2007. A comparison of a quasi-perpendicular method of absolute palaeointensity determination with other thermal and microwave techniques, 257, 564–581. https://doi.org/10.1016/j.epsl.2007.03.016

Biggin, A.J., Piispa, E.J., Pesonen, L.J., Holme, R., Paterson, G.A., Veikkolainen, T., Tauxe, L., 2015. Palaeomagnetic field intensity variations suggest Mesoproterozoic inner-core nucleation. Nature 526, 245–248. https://doi.org/10.1038/nature15523

Biggin, A.J., Poidras, T., 2006. First-order symmetry of weak-field partial thermoremanence in multi-domain ferromagnetic grains. 1. Experimental

827 evidence and physical implications. Earth Planet. Sci. Lett. 245, 438–453.
828 https://doi.org/10.1016/j.epsl.2006.02.035
829 Calvo-Rathert, M., Bógalo, M.F., Gogichaishvili, A., Sologashvili, J., Vashakidze, G.,
830 2013. New paleomagnetic and paleointensity data from Pliocene lava flows from
831 the Lesser Caucasus. J. Asian Earth Sci. 73, 347–361.
832 https://doi.org/10.1016/j.jseaes.2013.04.039
833 Calvo-Rathert, M., Morales-Contreras, J., Carrancho, Á., Goguitchaichvili, A., 2016. A
834 comparison of Thellier-type and multispecimen paleointensity determinations on
835 Pleistocene and historical lava flows from Lanzarote (Canary Islands, Spain).
836 Geochemistry, Geophys. Geosystems 17, 3638–3654.
837 https://doi.org/10.1002/2016GC006396
838 Cromwell, G., Tauxe, L., Staudigel, H., Ron, H., 2015. Paleointensity estimates from
839 historic and modern Hawaiian lava flows using glassy basalt as a primary source
840 material. Phys. Earth Planet. Inter. 241, 44–56.
841 https://doi.org/10.1016/j.pepi.2014.12.007
842 de Groot, L. V., Béguin, A., Kosters, M.E., van Rijsingen, E.M., Struijk, E.L.M., Biggin,
843 A.J., Hurst, E.A., Langereis, C.G., Dekkers, M.J., 2015. High paleointensities for the
844 Canary Islands constrain the Levant geomagnetic high. Earth Planet. Sci. Lett. 419,
845 154–167. https://doi.org/10.1016/j.epsl.2015.03.020
846 de Groot, L. V., Biggin, A.J., Dekkers, M.J., Langereis, C.G., Herrero-Bervera, E., 2013.
847 Rapid regional perturbations to the recent global geomagnetic decay revealed by
848 a new hawaiian record. Nat. Commun. 4, 1–7.
849 https://doi.org/10.1038/ncomms3727
850 de Groot, L. V., Dekkers, M.J., Mullender, T.A.T., 2012. Exploring the potential of
851 acquisition curves of the anhysteretic remanent magnetization as a tool to detect
852 subtle magnetic alteration induced by heating. Phys. Earth Planet. Inter. 194–195,
853 71–84. https://doi.org/10.1016/j.pepi.2012.01.006
854 de Groot, L. V., Dekkers, M. J., Visscher, M., and Ter Maat, G. W., 2014. Magnetic
855 properties and paleointensities as function of depth in a Hawaiian lava flow.
856 Geochemistry, Geophysics, Geosystems, 15(4), 1096–1112.
857 https://doi.org/10.1002/2013GC005094
858 de Groot, L. V., Pimentel, A., Di Chiara, A., 2016. The multimethod palaeointensity
859 approach applied to volcanics from Terceira: Full-vector geomagnetic data for the
860 past 50 kyr. Geophys. J. Int. 206, 590–604. https://doi.org/10.1093/gji/ggw095
861 Dekkers, M.J., Böhnel, H.N., 2006. Reliable absolute palaeointensities independent of
862 magnetic domain state. Earth Planet. Sci. Lett. 248, 507–516.
863 https://doi.org/10.1016/j.epsl.2006.05.040
864 Dunlop, D.J., 2011. Physical basis of the Thellier–Thellier and related paleointensity
865 methods. Phys. Earth Planet. Inter. 187, 118–138.
866 https://doi.org/10.1016/j.pepi.2011.03.006
867 Dunlop, D. J. and Özdemir, Ö., 2000. Effect of grain size and domain state on thermal
868 demagnetization tails. Geophysical Research Letters, 27(9), 1311–1314.
869 https://doi.org/10.1029/1999GL008461
870 Fabian, K. and Leonhardt, R., 2010. Multiple-specimen absolute paleointensity
871 determination: An optimal protocol including pTRM normalization, domain-state
872 correction, and alteration test. Earth Planet. Sci. Lett. 297, 84–94.
873 https://doi.org/10.1016/j.epsl.2010.06.006

Fabian, K. and Leonhardt, R., 2007. Theoretical analysis and experimental tests of multiple specimen absolute paleointensity determination techniques, in: Geophysical Research Abstracts. p. 04510.

Fanjat, G., 2012. *Les fluctuations du champ magnétique terrestre : des variations séculaires récentes aux renversements*. PhD. Géosciences, Universié de Montpellier. 768 p. Retrieved from https://tel.archives-ouvertes.fr/tel-00719380/PDF/thesefanjat2012.pdf

Haggerty, S.E., 1991. Oxide Textures: A Mini-Atlas, in: Lindsley, D.H. (Ed.), Oxide Minerals: Petrologic and Magnetic Significance, Rev. Mineral., Vol. 25. Mineral. Soc. of Am., Washington, D. C., pp. 129–137.

Herrero-Bervera, E., Valet, J.-P.P., 1999. Paleosecular variation during sequential geomagnetic reversals from Hawaii. Earth Planet. Sci. Lett. 171, 139–148. https://doi.org/10.1016/S0012-821X(99)00145-4

Kissel, C. and Laj, C., 2004. Improvements in procedure and paleointensity selection criteria (PICRIT-03) for Thellier and Thellier determinations: Application to Hawaiian basaltic long cores. Physics of the Earth and Planetary Interiors, 147(2–3 SPEC.ISS.), 155–169. https://doi.org/10.1016/j.pepi.2004.06.010

Laj, C. and Channell, J.E.T., 2007. Geomagnetic Excursions, in: Treatise on Geophysics. Elsevier, pp. 373–416. https://doi.org/10.1016/B978-044452748-6.00095-X

Lebedev, V.A., 2015. Geological map of Javakheti volcanic area (Lesser Caucasus), 1/200000, (2015). https://doi.org/10.13140/RG.2.1. 610 2359.2169

Lebedev, V.A., Bubnov, S.N., Dudauri, O.Z., Vashakidze, G.T., 2008. Geochronology of Pliocene volcanism in the Dzhavakheti Highland (the Lesser Caucasus). Part 1: Western part of the Dzhavakheti Highland. Stratigr. Geol. Correl. 16, 204–224. https://doi.org/10.1134/S0869593808020081

Leonhardt, R., Heunemann, C., and Krasa, D., 2004. Analyzing absolute paleointensity determinations: Acceptance criteria and the software ThellierTool4.0. Geochemistry, Geophysics, Geosystems, 5(12), 1–11. https://doi.org/10.1029/2004GC000807

Maisuradze, G.M., Kuloshvili, S.I., 1999. “Some Geological Problems of Late Volcanism in the Dzhavakheti Upland.” Tr. GIN AN Gruz. Nov. Ser. 114, 220–228.

Michalk, D.M., Biggin, A.J., Knudsen, M.F., Böhnel, H.N., Nowaczyk, N.R., Ownby, S., López-Martínez, M., 2010. Application of the multispecimen palaeointensity method to Pleistocene lava flows from the Trans-Mexican Volcanic Belt. Phys. Earth Planet. Inter. 179, 139–156. https://doi.org/10.1016/j.pepi.2010.01.005

Michalk, D.M., Muxworthy, A.R., Böhnel, H.N., Maclennan, J., Nowaczyk, N., Harald, N.B., Maclennan, J., Nowaczyk, N., 2008. Evaluation of the multispecimen parallel differential pTRM method: A test on historical lavas from Iceland and Mexico. Geophys. J. Int. 173, 409–420. https://doi.org/10.1111/j.1365-246X.2008.03740.x

Monster, M.W.L., de Groot, L. V., Biggin, A.J., Dekkers, M.J., 2015. The performance of various palaeointensity techniques as a function of rock magnetic behaviour - A case study for La Palma. Phys. Earth Planet. Inter. 242, 36–49. https://doi.org/10.1016/j.pepi.2015.03.004

Monster, M.W.L., de Groot, L. V., Dekkers, M.J., 2015. MSP-Tool: A VBA-Based Software Tool for the Analysis of Multispecimen Paleointensity Data. Front. Earth Sci. 3, 1–9. https://doi.org/10.3389/feart.2015.00086

Monster, M.W.L., Langemeijer, J., Wiarda, L.R., Dekkers, M.J., Biggin, A.J., Hurst, E.A.,

Groot, L.V. d., 2018. Full-vector geomagnetic field records from the East Eifel, Germany. Phys. Earth Planet. Inter. 274, 148–157. https://doi.org/10.1016/j.pepi.2017.11.009

Muxworthy, A.R., Taylor, S.N., 2011. Evaluation of the domain-state corrected multiple-specimen absolute palaeointensity protocol: a test of historical lavas from Iceland. Geophys. J. Int. 187, 118–127. https://doi.org/10.1111/j.1365-246X.2011.05163.x

Paterson, G. A., 2011. A simple test for the presence of multidomain behavior during paleointensity experiments. Journal of Geophysical Research: Solid Earth, 116(10), 1–12. https://doi.org/10.1029/2011JB008369

Paterson, G.A., Tauxe, L., Biggin, A.J., Shaar, R., Jonestrask, L.C., 2014. On improving the selection of Thellier-type paleointensity data. Geochemistry, Geophys. Geosystems 15, 1180–1192. https://doi.org/10.1002/2013GC005135

Paterson, G.A., Tauxe, L., Biggin, A.J., Shaar, R., Jonestrask, L.C., 2014. Standard Paleointensity Definitions v1.1 0–43.

Prévot, M., Mankinen, E.A., Coe, R.S., Grommé, C.S., 1985. The Steens Mountain (Oregon) geomagnetic polarity transition: 2. Field intensity variations and discussion of reversal models. J. Geophys. Res. Solid Earth 90, 10417–10448. https://doi.org/10.1029/JB090iB12p10417

Prevot, M., Mankinen, E.A., Gromme, C.S., Coe, R.S., 1985. How the geomagnetic field vector reverses polarity. Nature 316, 230–234. https://doi.org/10.1038/316230a0

Riisager, J., Perrin, M., Riisager, P., Ruffet, G., 2000. Paleomagnetism, paleointensity and geochronology of Miocene basalts and baked sediments from Velay Oriental, French Massif Central. J. Geophys. Res. Solid Earth 105, 883–896. https://doi.org/10.1029/1999JB900337

Sánchez-Moreno, E.M., 2018. Variation of the absolute paleointensity of the Earth's magnetic field recorded in sequences of basaltic flows from the volcanic region of Djavakheti (Georgia). PhD. Universidad de Burgos. 376p. doi:10.13140/RG.2.2.30939.00804

Sánchez-Moreno, E. M., Calvo-Rathert, M., Goguitchaichvili, A., Tauxe, L., Vashakidze, G. T., Lebedev, V. A. (2020). Weak palaeointensity results over a Pliocene volcanic sequence from Lesser Caucasus (Georgia): transitional record or time averaged field? Geophysical Journal International, 220(3), 1604–1618. https://doi.org/10.1093/gji/ggz533

Sánchez-Moreno, E.M., Calvo-Rathert, M., Goguitchaichvili, A., Vashakidze, G.T., Lebedev, V.A., 2018. Evidence of Unusual Geomagnetic Regimes Recorded in Plio-Pleistocene Volcanic Sequences from the Lesser Caucasus (Southern Georgia). Geochemistry, Geophys. Geosystems 19, 1–18. https://doi.org/10.1029/2017GC007358

Sato, M., Yamamoto, Y., Nishioka, T., Kodama, K., Mochizuki, N., Tsunakawa, H., 2016. Hydrostatic pressure effect on magnetic hysteresis parameters of pseudo-single-domain magnetite. Geochemistry, Geophys. Geosystems 17, 2825–2834. https://doi.org/10.1002/2016GC006406

Selkin, P. A., and Tauxe, L., 2000. Long-term variations in palaeointensity. Philosophical Transactions of the Royal Society A: Mathematical, Physical and Engineering Sciences, 358(1768), 1065–1088. https://doi.org/10.1098/rsta.2000.0574

Tauxe, L., 2006. Long-term trends in paleointensity: The contribution of DSDP/ODP

submarine basaltic glass collections. Phys. Earth Planet. Inter. 156, 223–241. https://doi.org/10.1016/j.pepi.2005.03.022

Tauxe, L., Shaar, R., Jonestrask, L., Swanson-Hysell, N.L., Minnett, R., Koppers, A.A.P., Constable, C.G., Jarboe, N., Gaastra, K., Fairchild, L., 2016. PmagPy: Software package for paleomagnetic data analysis and a bridge to the Magnetics Information Consortium (MagIC) Database. Geochemistry, Geophys. Geosystems 17, 2450–2463. https://doi.org/10.1002/2016GC006307

Tauxe, L., Staudigel, H., 2004. Strength of the geomagnetic field in the cretaceous normal superchron: New data from submarine basaltic glass of the troodos ophiolite. Geochemistry, Geophys. Geosystems 5, 223–241. https://doi.org/10.1029/2003GC000635

Tema, E., Camps, P., Ferrara, E., Poidras, T., Nazionale, F.I., Metrologica, R., Tema, E., Camps, P., Ferrara, E., Poidras, T., 2015. Directional results and absolute archaeointensity determination by the classical Thellier and the multi-specimen DSC protocols for two kilns excavated at Osterietta, Italy. Stud. Geophys. Geod. 59, 554–577. https://doi.org/10.1007/s11200-015-0413-0

Tema, E., Ferrara, E., Camps, P., Conati, C., Spatafora, S., Carvallo, C., Poidras, T., Conati Barbaro, C., Spatafora, S., Carvallo, C., Poidras, T., 2016. The Earth ' s magnetic field in Italy during the Neolithic period : New data from the Early Neolithic site of Portonovo (Marche , Italy). Earth Planet. Sci. Lett. 448, 49–61. https://doi.org/10.1016/j.epsl.2016.05.003

Thellier, E., Thellier, O., 1959. Sur líntensité du champ magnétique terrestre dans le passé historique et géologique. Ann. Geophys. 15, 285–376.

Yu, Y., Tauxe, L., Genevey, A., 2004. Toward an optimal geomagnetic field intensity determination technique. Geochemistry, Geophys. Geosystems 5, n/a-n/a. https://doi.org/10.1029/2003GC000630

Table 1. *Paleointensity determinations obtained with the multispecimen methods (Biggin and Poidras, 2006; Dekkers and Böhnel, 2006; Fabian and Leonhardt, 2010).*

Site	Spec.	Prot.	N	n	R^2	f	B (μT)	CI_{95} (μT)	$CI_{95\ T/2}$ (μT)	$CI_{95\ (T/2)\%}$ (%)	ΔB (μT)	ΔB (%)	ε_{alt} (%)	Class
AP01	03A/04A	DB	8	6	0.9994	-	57.4	[56.8 58.0]	0.6	1.0				B
		FC	8	7	0.9928	0.33-0.53	55.2	[53.2 57.0]	1.9	3.4				
		DSC	8	7	0.9814	0.33-0.53	45.1	[43.1 47.2]	2.1	4.5	7.6	16.9	15.2	B
AP03	04A	DB	8	8	0.9968	-	28.6	[27.8 29.4]	0.8	2.8				B*
		FC	8	7	0.9981	0.21-0.32	27.7	[26.4 28.7]	1.2	4.2				
		DSC	8	6	0.9957	0.21-0.32	22.0	[21.2 23.1]	1.0	4.3	6.7	30.4	15.7	B*
AP04	03BI/AII	DB	7	7	0.9859	-	67.1	[63.1 70.5]	3.7	5.5				B
		FC	4	3	0.9958	0.38-0.46	63.7	[58.5 71.5]	6.5	10.2				
		DSC	4	4	0.9893	0.38-0.46	55.4	[50.7 61.8]	5.6	10.0	9.7	17.6	11.0	B
AP05	01B	DB	7	5	0.9406	-	117.5	[70.3 158.6]	43.9	37.3				-
		FC	4	4	0.8563	0.21-0.32	151.0	[-670.0 885.6]	777.8	515.1				
		DSC	4	3	0.9991	0.21-0.32	100.4	[96.9 104.2]	3.6	3.5	23.7	23.6	5.4	B
AP10	04A	DB	8	8	0.9935	-	32.4	[30.9 33.6]	1.4	4.2				B
		FC	8	6	0.9909	0.34-0.44	31.1	[27.2 33.9]	3.4	10.8				
		DSC	8	6	0.9938	0.30-0.44	25.5	[23.5 27.2]	1.9	7.3	3.9	15.1	10.7	B
AP11	02A	DB	8	8	0.9687	-	21.9	[16.7 27.4]	5.4	24.4				-
		FC	8	6	0.9886	0.11-0.19	20.0	[17.5 21.9]	2.2	11.0				
		DSC	8	6	0.9971	0.11-0.19	15.7	[15.1 16.3]	0.6	3.8	4.7	30.0	9.5	T^{v}
AP12	07BII/CII	DB	7	6	0.7872	-	46.4	[-258.5 336.0]	297.3	640.6				-
		FC	4	3	0.9988	0.24-0.35	49.9	[47.7 52.0]	2.2	4.3				
		DSC	4	4	0.9830	0.24-0.35	36.8	[30.9 41.6]	5.4	14.5	6.3	17.2	7.2	A
AP14	06B	DB	7	6	0.9858	-	13.6	[10.4 17.3]	3.5	25.4				B
		FC	4	4	0.9998	0.47-0.48	14.4	[14.1 14.6]	0.3	1.7				
		DSC	4	4	0.9992	0.47-0.48	14.0	[13.5 14.4]	0.5	3.2	0.5	3.7	2.6	A
AP15	07A/BII	DB	7	5	0.4624	-	52.8	[-12.2 131.3]	71.8	135.9				-
		FC	4	3	0.9649	0.10-0.18	27.1	[10.5 36.6]	13.1	48.2				
		DSC	4	3	0.9493	0.10-0.18	27.2	[18.0 34.5]	8.3	30.3	0.3	1.2	3.6	T^{v}
AP17	06AII/BII	DB	7	6	0.9825	-	26.6	[24.8 28.2]	1.7	6.4				B
		FC	5	3	0.9953	0.24-0.33	28.1	[25.6 30.9]	2.7	9.4				
		DSC	5	3	0.9965	0.24-0.33	22.6	[21.0 24.2]	1.6	7.1	5.9	26.2	8.4	B

AP19	01BII/CII	DB	7	6	0.9946	-	26.2	[25.3 27.0]	0.9	3.2				-
		FC	5	4	0.9931	0.07-0.14	24.2	[20.8 26.7]	3.0	12.2				
		DSC	5	5	0.9784	0.07-0.14	19.2	[16.3 21.8]	2.8	14.3	3.7	19.4	3.4	T^v
AP20	07B/09C	DB	8	7	0.9381	-	4.1	[-10.9 23.5]	17.2	423.6				-
		FC	8	4	0.9914	0.26-0.32	14.6	[13.4 16.3]	1.5	9.9				
		DSC	8	4	0.9593	0.26-0.32	11.0	[9.05 13.7]	2.3	21.1	5.6	51.1	35.4	T^v

Note. Site: Lava flow name. Spec.: Specimen sub-name. Prot.: MSP type protocol. N: Number specimens with different B_{lab} applied in the experiment. n: Number specimens with different B_{lab} used in the determination. Experimental statistics: R^2, f, CI_{95} T/2, CI_{95} (T/2)% , ΔB and ε_{alt} (Table S2). B: Paleointensity. Class: Determination quality level. Tv: Determinations that have not passed selection criteria, but their agreement with Thellier-type results has driven us to consider them for final paleointensity calculations.

Table 2. *Paleointensity averaged for each lava flow and for each the absolute paleointensity determination method.*

	TT				IZZI				MSP-DB				MSP-FC				MSP-DSC			
Site	n	B (μT)	σB (μT)	σB (%)	n	B (μT)	σB (μT)	σB (%)	n	B (μT)	95% CI (μT)	95% $CI_{T/2}$ (%)	n	B (μT)	95% CI (μT)	95% $CI_{T/2}$ (%)	n	B (μT)	95% CI (μT)	95% $CI_{T/2}$ (%)
AP01	2	17.8	1.8	10.4	1	37.8	0.8	2.0	6	57.4	[56.8 - 58.0]	1.0	7	55.2	[53.2 - 57.0]	3.4	7	45.1	[43.1 - 47.2]	4.5
AP02	2	41.0	3.5	8.7	4	35.1	2.1	6.1												
AP04	3	33.5	8.4	25.0	4	34.1	1.7	5.1	7	67.1	[63.1 - 70.5]	5.5	3	63.7	[58.5 - 71.5]	10.2	4	55.4	[50.7 - 61.8]	10.0
AP05					4	29.9	7.3	19.5	5	117.5	[70.3 - 158.6]	37.3	4	151.0	[-670.0 - 885.6]	515.1	3	100.4	[96.9 - 104.2]	3.5
AP03	1	39.6	2.4	6.0					8	28.6	[27.8 - 29.4]	2.8	7	27.7	[26.4 - 28.7]	4.2	6	22.0	[21.2 - 23.1]	4.3
AP06					3	25.2	1.6	6.5												
AP07	1	12.9	0.5	4.0	2	19.6	0.5	2.6												
AP08	1	23.6	1.1	4.5																
AP09	3	16.6	0.7	4.4																
AP10	2	12.9	0.6	4.5					8	32.4	[30.9 - 33.6]	4.2	6	31.1	[27.2 - 33.9]	10.8	6	25.5	[23.5 - 27.2]	7.3
AP12	2	13.6	0.4	2.6					6	46.4	[-258.5 - 336.0]	640.6	3	49.9	[47.7 - 52.0]	4.3	4	36.8	[30.9 - 41.6]	14.5
AP11	2	20.3	3.1	15.5	4	24.9	4.6	18.3	8	21.9	[16.7 - 27.4]	24.4	6	20.0	[17.5 - 21.9]	11.0	6	15.7	[15.1 - 16.3]	3.8
AP13	1	13.0	0.7	5.0	2	12.2	0.2	1.4												
AP14	3	19.6	1.3	6.8	6	20.3	0.7	3.4	6	13.6	[10.4 - 17.3]	25.4	4	14.4	[14.1 - 14.6]	1.7	4	14.0	[13.5 - 14.4]	3.2
AP15	1	23.9	1.6	6.9					5	52.8	[-12.2 - 131.3]	135.9	3	27.1	[10.5 - 36.6]	48.2	3	27.2	[18.0 - 34.5]	30.3
AP16					5	16.8	2.3	13.9												
AP17	2	20.2	4.0	19.6	7	26.1	4.7	21.9	6	26.6	[24.8 - 28.2]	6.4	3	28.1	[25.6 - 30.9]	9.4	3	22.6	[21.0 - 24.2]	7.1
AP18	1	24.7	0.5	2.0	4	23.1	1.1	4.6												
AP20	2	16.4	1.9	11.8	3	16.8	0.8	4.7	7	4.1	[-10.9 - 23.5]	423.6	4	14.6	[13.4 - 16.3]	9.9	4	11.0	[9.1 - 13.7]	21.1
AP19	2	20.9	0.8	4.1	5	21.3	1.0	1.9	6	26.2	[25.3 - 27.0]	3.2	4	24.2	[20.8 - 26.7]	12.2	5	19.2	[16.3 - 21.8]	14.3

Note. All the paleointensities obtained by the multispecimen method are shown, although the quality criteria are not fulfilled.

Table 3. *Final weighted average paleointensities per lava flow in the Apnia sequence.*

age (Ma)	Site	Q	TT	IZZI	MSP DSC	Weighted average B (μT)	sd (μT)		sd (%)	VADM (10^{22} Am^2)	σVADM (10^{22} Am^2)
3.09	AP01	**1**	+	1	1	41.5	5.2		12.5	7.1	0.88
3.09	AP02	2	2	4	-	37.1	3.0		8.2	6.3	0.52
3.09	AP04	2	3	4	+	33.8	0.3		0.9	5.8	0.05
3.09	AP05	3	x	4	+	29.9	7.3	sd*	24.4	5.1	1.24
3.28	AP03	4	1	x	+	39.6	2.4	σPI	6.0	6.7	0.40
3.28	AP06	3	x	3	-	25.2	1.6	sd*	6.3	4.3	0.27
3.75	AP07	2	1	2	-	17.4	3.9		22.3	3.0	0.66
3.75	AP08	4	1	x	-	23.6	1.1	σPI	4.5	4.0	0.18
3.75	AP09	3	3	x	-	16.6	0.7	sd*	4.2	2.8	0.12
3.75	AP10	4	2	x	+	12.9	0.6	sd*	4.7	2.2	0.10
3.70	AP12	4	2	x	+	13.6	0.4	sd*	2.9	2.3	0.07
3.70	AP11	2	2	4	x	23.4 (22.3)	2.4 (3.6)		10.2 (16.3)	4.0 (3.8)	0.40 (0.61)
3.70	AP13	2	1	2	-	12.5	0.5		3.7	2.1	0.08
3.70	AP14	**1**	3	6	1	19.4	2.1		10.7	3.3	0.35
3.70	AP15	2	1	x	x	23.9 (25.6)	1.6 (2.3)	σPI	6.9 (9.1)	4.1 (4.4)	0.28 (0.39)
3.70	AP16	3	x	5	-	16.8	2.3	sd*	13.7	2.9	0.39
3.70	AP17	**1**	2	7	1	24.6	2.5		10.4	4.2	0.43
3.70	AP18	2	1	4	-	23.4	0.7		3.1	4.0	0.12
3.70	AP20	2	3	3	x	16.6 (16.0)	0.2 (2.0)		1.3	2.8 (2.7)	0.04 (0.34)
3.70	AP19	2	2	5	x	21.2 (20.9)	0.2 (0.7)		0.9 (3.5)	3.6 (3.6)	0.03 (0.12)

+	rejected by paleointensity value
x	rejected by quality criteria
-	not measured
σB	± single paleointensity determination error calculated from the Arai plot linear regression
sd*	standard deviation of the paleointensities obtained from a single lava flow
( )	averaged paleointensity calculated with MSP-DSC of bad quality match with Thellier results

Note. Final weighted paleointensity average calculated by lava flow using the number of individual determinations (note that in the case of multispecimen determinations, although several specimens are used for a single determination the weighted value remains equal to 1). The number of determinations performed with each method is shown. Those methods rejected by paleointensity value, or quality criteria or those not measured are indicated. Q: quality paleointensity average level. TT: Thellier-Thellier (1959); IZZI: In-field/Zero-field protocol (Yu et al., 2004); MSP-DSC: Multispecimen domain-state correction (Fabian and Leonhardt, 2010); *sd (μT and %)*: standard deviation by lava flow (see table for especial cases). VADM: Virtual axial dipole moment. σVADM: Virtual axial dipole moment error calculated from *sd* (μT).

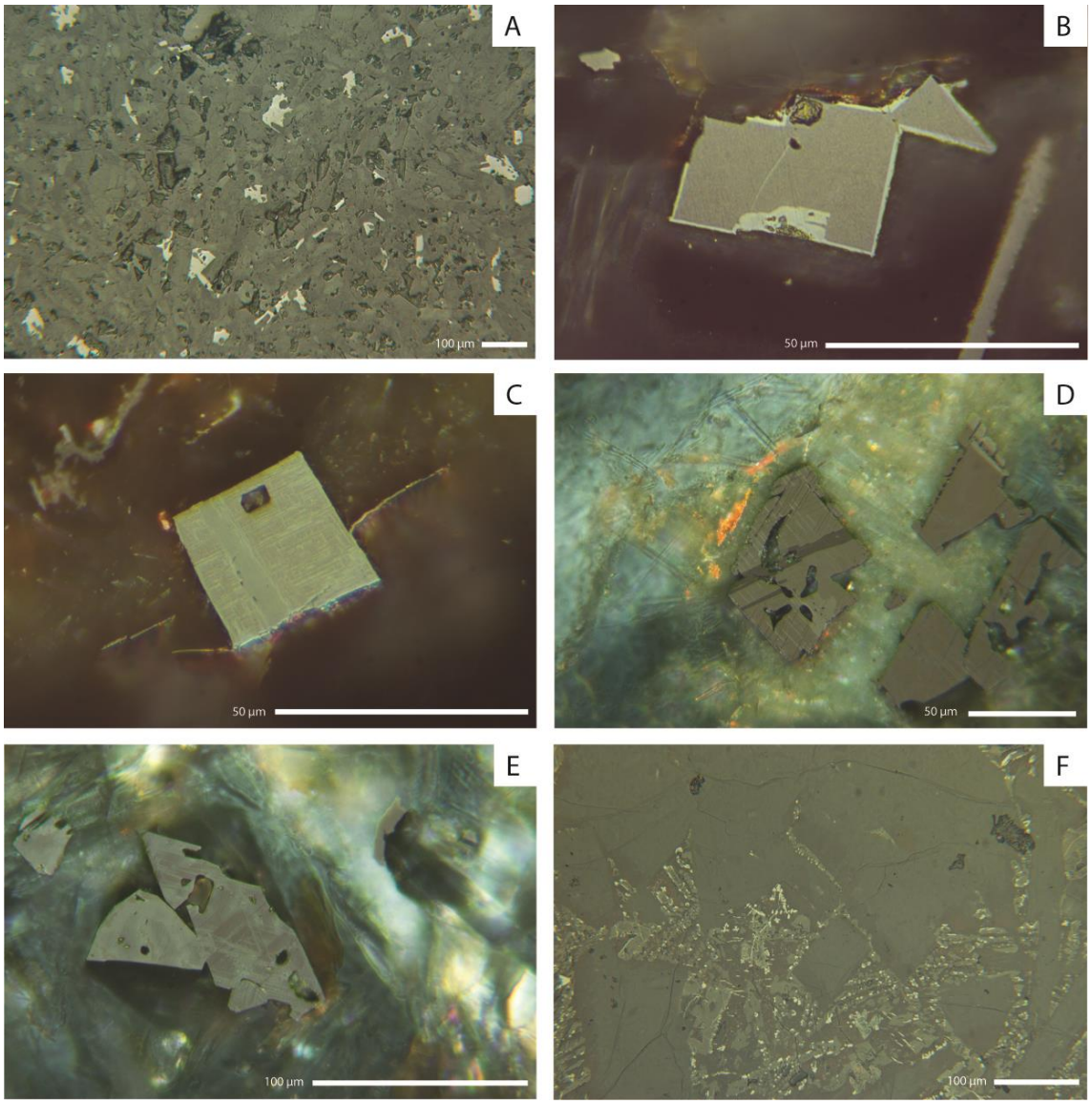

Figure 1. Reflected light optical microscope images of polished thin sections from the Apnia sequence. (a) Overview image of the AP02 sample showing the distribution of euhedral to subhedral crystals. (b) Detailed image of a titanite crystal from AP06 with maghemitization on the crystal edges. (c) and (d) Euhedral titanomagnetite crystal from AP13 with Trellis and Sandwich intergrowths of ilmenite, indicative of C3 oxidation stage. (e) Titanomagnetite crystal with Trellis ilmenite intergrowths pointing out a C3 oxidation stage (AP06). (f) Detailed view of micron-sized titanomagnetite crystals disseminated in AP14.

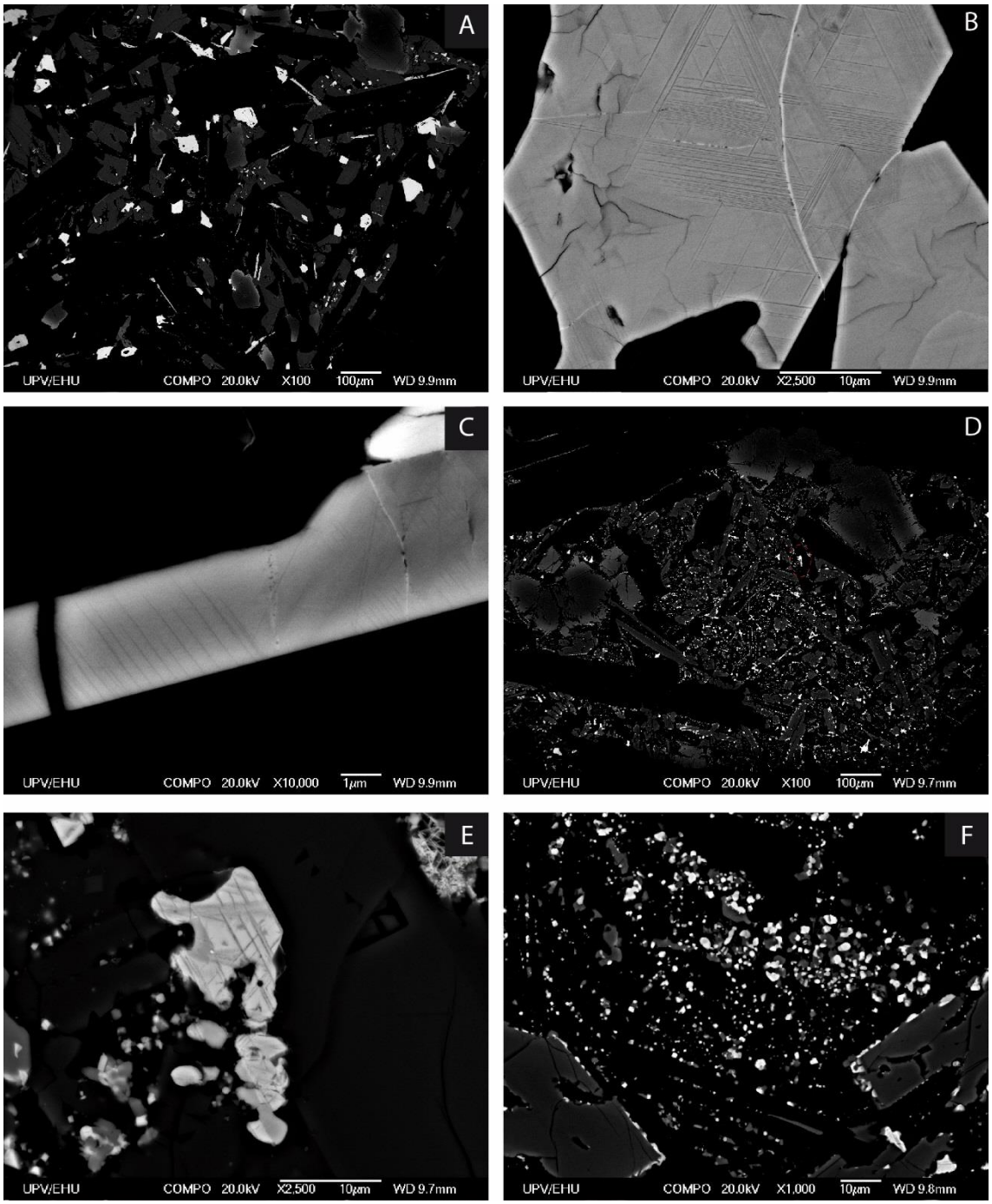

Figure 2. Scanning electron microscope (SEM) images of polished thin sections from the Apnia sequence. (a) Overview image of the AP06 sample showing the distribution of euhedral to subhedral crystals. (b) Detailed image of a titanite crystal from AP06 with Trellis intergrowths of ilmenite, indicative of C3 oxidation stage, and micro-cracks around the crystal boundaries due to maghemitization. (c) Detail of an acicular ilmenite crystal showing exsolved rutile needles, evidence of R2 oxidation stage. Sample AP06. (d) General view of the sample AP08 showing the small size and skeletal morphologies of the opaque minerals. The dash-red circle indicates the crystal of image (e). (e) Titanomagnetite crystal with Trellis and Sandwich ilmenite intergrowths pointing out a C3 oxidation stage (AP08). (f) Detailed view of micron-sized titanomagnetite crystals disseminated in AP08.

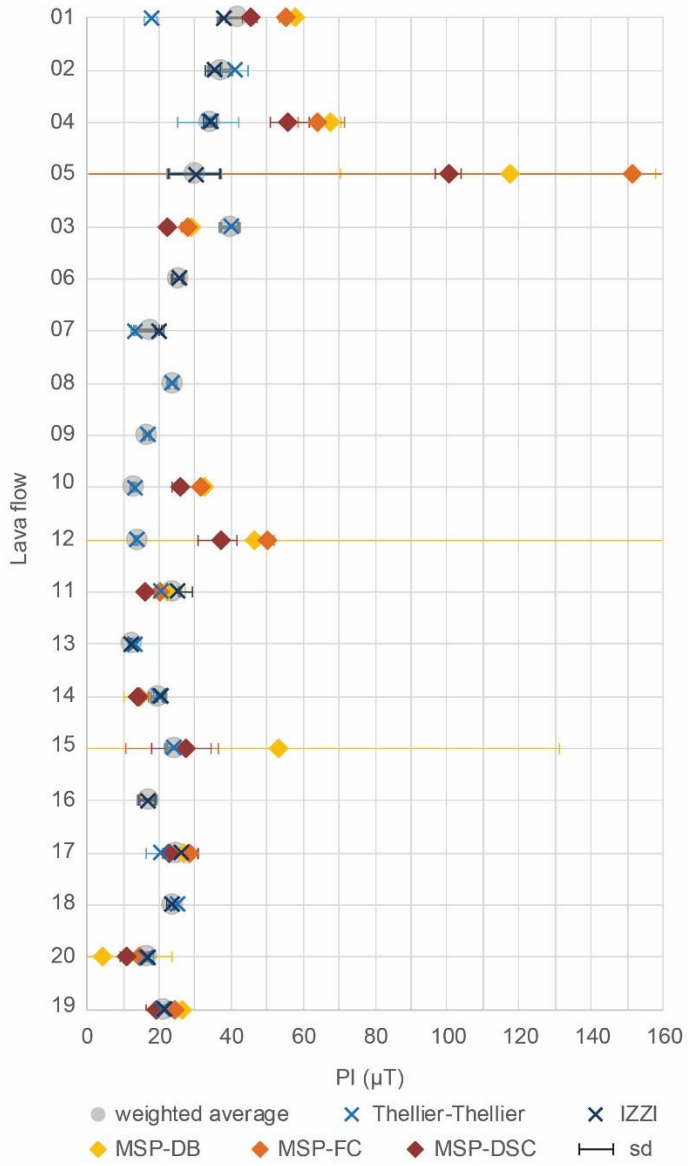

Figure 3. Final weighted average paleointensities per lava flow in the Apnia sequence. TT: Thellier-Thellier (1959); IZZI: In-field Zero-field protocol (Yu et al., 2004); MSP-DB: Multispecimen parallel differential pTRM method (Biggin and Poidras, 2006; Dekkers and Böhnel, 2006); MSP-FC: Multispecimen with fraction correction (Fabian and Leonhardt, 2010); MSP-DSC: Multispecimen with domain-state correction (Fabian and Leonhardt, 2010); sd: standard deviation.

Site	Spec.	Prot.	N	n	R^2	f	B (μT)	CI_{95} (μT)	$CI_{95\ T/2}$ (μT)	$CI_{95\ (T/2)\%}$ (%)	ΔB (μT)	ΔB (%)	ε_{alt} (%)	Class
AP01	03A/04A	DB	8	6	0.9994	-	57.4	[56.8 58.0]	0.6	1.0				B
		FC	8	7	0.9928	0.33-0.53	55.2	[53.2 57.0]	1.9	3.4				
		DSC	8	7	0.9814	0.33-0.53	45.1	[43.1 47.2]	2.1	4.5	7.6	16.9	15.2	B
AP03	04A	DB	8	8	0.9968	-	28.6	[27.8 29.4]	0.8	2.8				B*
		FC	8	7	0.9981	0.21-0.32	27.7	[26.4 28.7]	1.2	4.2				
		DSC	8	6	0.9957	0.21-0.32	22.0	[21.2 23.1]	1.0	4.3	6.7	30.4	15.7	B*
AP04	03BI/AII	DB	7	7	0.9859	-	67.1	[63.1 70.5]	3.7	5.5				B
		FC	4	3	0.9958	0.38-0.46	63.7	[58.5 71.5]	6.5	10.2				
		DSC	4	4	0.9893	0.38-0.46	55.4	[50.7 61.8]	5.6	10.0	9.7	17.6	11.0	B
AP05	01B	DB	7	5	0.9406	-	117.5	[70.3 158.6]	43.9	37.3				-
		FC	4	4	0.8563	0.21-0.32	151.0	[-670.0 885.6]	777.8	515.1				
		DSC	4	3	0.9991	0.21-0.32	100.4	[96.9 104.2]	3.6	3.5	23.7	23.6	5.4	B
AP10	04A	DB	8	8	0.9935	-	32.4	[30.9 33.6]	1.4	4.2				B
		FC	8	6	0.9909	0.34-0.44	31.1	[27.2 33.9]	3.4	10.8				
		DSC	8	6	0.9938	0.30-0.44	25.5	[23.5 27.2]	1.9	7.3	3.9	15.1	10.7	B
AP11	02A	DB	8	8	0.9687	-	21.9	[16.7 27.4]	5.4	24.4				-
		FC	8	6	0.9886	0.11-0.19	20.0	[17.5 21.9]	2.2	11.0				
		DSC	8	6	0.9971	0.11-0.19	15.7	[15.1 16.3]	0.6	3.8	4.7	30.0	9.5	T^v
AP12	07BII/CII	DB	7	6	0.7872	-	46.4	[-258.5 336.0]	297.3	640.6				-
		FC	4	3	0.9988	0.24-0.35	49.9	[47.7 52.0]	2.2	4.3				
		DSC	4	4	0.9830	0.24-0.35	36.8	[30.9 41.6]	5.4	14.5	6.3	17.2	7.2	A
AP14	06B	DB	7	6	0.9858	-	13.6	[10.4 17.3]	3.5	25.4				B
		FC	4	4	0.9998	0.47-0.48	14.4	[14.1 14.6]	0.3	1.7				
		DSC	4	4	0.9992	0.47-0.48	14.0	[13.5 14.4]	0.5	3.2	0.5	3.7	2.6	A
AP15	07A/BII	DB	7	5	0.4624	-	52.8	[-12.2 131.3]	71.8	135.9				-
		FC	4	3	0.9649	0.10-0.18	27.1	[10.5 36.6]	13.1	48.2				
		DSC	4	3	0.9493	0.10-0.18	27.2	[18.0 34.5]	8.3	30.3	0.3	1.2	3.6	T^v
AP17	06AII/BII	DB	7	6	0.9825	-	26.6	[24.8 28.2]	1.7	6.4				B
		FC	5	3	0.9953	0.24-0.33	28.1	[25.6 30.9]	2.7	9.4				
		DSC	5	3	0.9965	0.24-0.33	22.6	[21.0 24.2]	1.6	7.1	5.9	26.2	8.4	B
AP19	01BII/CII	DB	7	6	0.9946	-	26.2	[25.3 27.0]	0.9	3.2				-
		FC	5	4	0.9931	0.07-0.14	24.2	[20.8 26.7]	3.0	12.2				
		DSC	5	5	0.9784	0.07-0.14	19.2	[16.3 21.8]	2.8	14.3	3.7	19.4	3.4	T^v
AP20	07B/09C	DB	8	7	0.9381	-	4.1	[-10.9 23.5]	17.2	423.6				-
		FC	8	4	0.9914	0.26-0.32	14.6	[13.4 16.3]	1.5	9.9				
		DSC	8	4	0.9593	0.26-0.32	11.0	[9.05 13.7]	2.3	21.1	5.6	51.1	35.4	T^v

	TT				IZZI				MSP-DB				MSP-FC		
Site	n	B (μT)	σB (μT)	σB (%)	n	B (μT)	σB (μT)	σB (%)	n	B (μT)	95% CI (μT)	95% $CI_{T/2}$ (%)	n	B (μT)	95% CI (μT)
AP01	2	17.8	1.8	10.4	1	37.8	0.8	2.0	6	57.4	[56.8 - 58.0]	1.0	7	55.2	[53.2 - 57.0]
AP02	2	41.0	3.5	8.7	4	35.1	2.1	6.1							
AP04	3	33.5	8.4	25.0	4	34.1	1.7	5.1	7	67.1	[63.1 - 70.5]	5.5	3	63.7	[58.5 - 71.5]
AP05					4	29.9	7.3	19.5	5	117.5	[70.3 - 158.6]	37.3	4	151.0	[-670.0 - 885.6]
AP03	1	39.6	2.4	6.0					8	28.6	[27.8 - 29.4]	2.8	7	27.7	[26.4 - 28.7]
AP06					3	25.2	1.6	6.5							
AP07	1	12.9	0.5	4.0	2	19.6	0.5	2.6							
AP08	1	23.6	1.1	4.5											
AP09	3	16.6	0.7	4.4											
AP10	2	12.9	0.6	4.5					8	32.4	[30.9 - 33.6]	4.2	6	31.1	[27.2 - 33.9]
AP12	2	13.6	0.4	2.6					6	46.4	[-258.5 - 336.0]	640.6	3	49.9	[47.7 - 52.0]
AP11	2	20.3	3.1	15.5	4	24.9	4.6	18.3	8	21.9	[16.7 - 27.4]	24.4	6	20.0	[17.5 - 21.9]
AP13	1	13.0	0.7	5.0	2	12.2	0.2	1.4							
AP14	3	19.6	1.3	6.8	6	20.3	0.7	3.4	6	13.6	[10.4 - 17.3]	25.4	4	14.4	[14.1 - 14.6]
AP15	1	23.9	1.6	6.9					5	52.8	[-12.2 - 131.3]	135.9	3	27.1	[10.5 - 36.6]
AP16					5	16.8	2.3	13.9							
AP17	2	20.2	4.0	19.6	7	26.1	4.7	21.9	6	26.6	[24.8 - 28.2]	6.4	3	28.1	[25.6 - 30.9]
AP18	1	24.7	0.5	2.0	4	23.1	1.1	4.6							
AP20	2	16.4	1.9	11.8	3	16.8	0.8	4.7	7	4.1	[-10.9 - 23.5]	423.6	4	14.6	[13.4 - 16.3]
AP19	2	20.9	0.8	4.1	5	21.3	1.0	1.9	6	26.2	[25.3 - 27.0]	3.2	4	24.2	[20.8 - 26.7]

95% $CI_{T/2}$ (%)	n	MSP-DSC B (μT)	95% CI (μT)	95% $CI_{T/2}$ (%)
3.4	7	45.1	[43.1 - 47.2]	4.5
10.2	4	55.4	[50.7 - 61.8]	10.0
515.1	3	100.4	[96.9 - 104.2]	3.5
4.2	6	22.0	[21.2 - 23.1]	4.3
10.8	6	25.5	[23.5 - 27.2]	7.3
4.3	4	36.8	[30.9 - 41.6]	14.5
11.0	6	15.7	[15.1 - 16.3]	3.8
1.7	4	14.0	[13.5 - 14.4]	3.2
48.2	3	27.2	[18.0 - 34.5]	30.3
9.4	3	22.6	[21.0 - 24.2]	7.1
9.9	4	11.0	[9.1 - 13.7]	21.1
12.2	5	19.2	[16.3 - 21.8]	14.3

age (Ma)	Site	Q	TT	IZZI	MSP DSC	Weighted average B (µT)	sd (µT)		sd (%)	VADM (10^{22} Am^2)	σVADM (10^{22} Am^2)
3.09	AP01	**1**	+	1	1	41.5	5.2		12.5	7.1	0.88
3.09	AP02	2	2	4	-	37.1	3.0		8.2	6.3	0.52
3.09	AP04	2	3	4	+	33.8	0.3		0.9	5.8	0.05
3.09	AP05	3	x	4	+	29.9	7.3	sd*	24.4	5.1	1.24
3.28	AP03	4	1	x	+	39.6	2.4	σPI	6.0	6.7	0.40
3.28	AP06	3	x	3	-	25.2	1.6	sd*	6.3	4.3	0.27
3.75	AP07	2	1	2	-	17.4	3.9		22.3	3.0	0.66
3.75	AP08	4	1	x	-	23.6	1.1	σPI	4.5	4.0	0.18
3.75	AP09	3	3	x	-	16.6	0.7	sd*	4.2	2.8	0.12
3.75	AP10	4	2	x	+	12.9	0.6	sd*	4.7	2.2	0.10
3.70	AP12	4	2	x	+	13.6	0.4	sd*	2.9	2.3	0.07
3.70	AP11	2	2	4	x	23.4 (22.3)	2.4 (3.6)		10.2 (16.3)	4.0 (3.8)	0.40 (0.61)
3.70	AP13	2	1	2	-	12.5	0.5		3.7	2.1	0.08
3.70	AP14	**1**	3	6	1	19.4	2.1		10.7	3.3	0.35
3.70	AP15	2	1	x	x	23.9 (25.6)	1.6 (2.3)	σPI	6.9 (9.1)	4.1 (4.4)	0.28 (0.39)
3.70	AP16	3	x	5	-	16.8	2.3	sd*	13.7	2.9	0.39
3.70	AP17	**1**	2	7	1	24.6	2.5		10.4	4.2	0.43
3.70	AP18	2	1	4	-	23.4	0.7		3.1	4.0	0.12
3.70	AP20	2	3	3	x	16.6 (16.0)	0.2 (2.0)		1.3	2.8 (2.7)	0.04 (0.34)
3.70	AP19	2	2	5	x	21.2 (20.9)	0.2 (0.7)		0.9 (3.5)	3.6 (3.6)	0.03 (0.12)

+	rejected by paleointensity value
x	rejected by quality criteria
-	not measured
σB	± single paleointensity determination error calculated from the Arai plot linear regression
sd*	standard deviation of the paleointensities obtained from a single lava flow
( )	averaged paleointensity calculated with MSP-DSC of bad quality match with Thellier results

Figure 1.

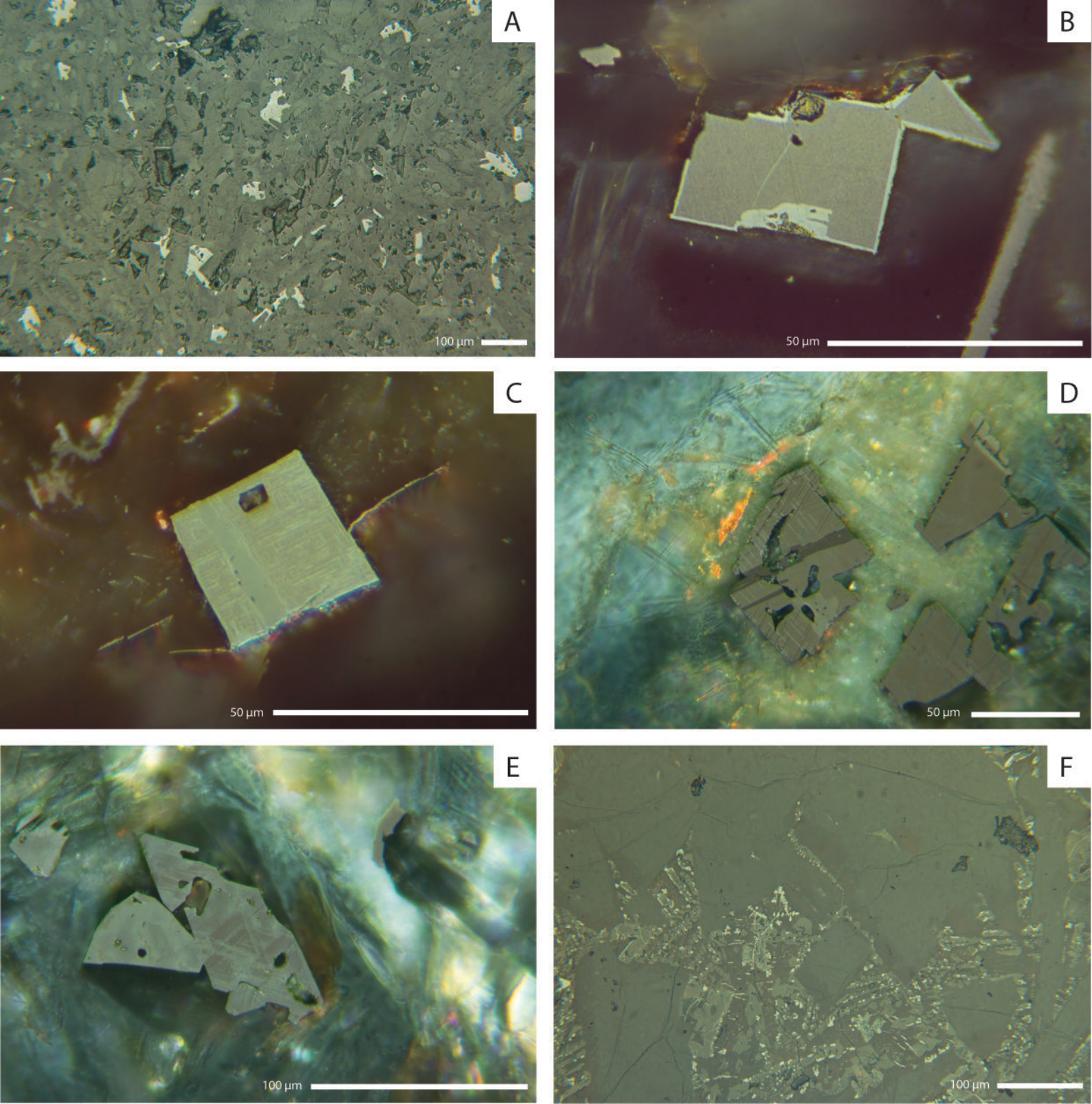
A
100 µm
B
50 µm
C
50 µm
D
50 µm
E
100 µm
F
100 µm

Figure 2.

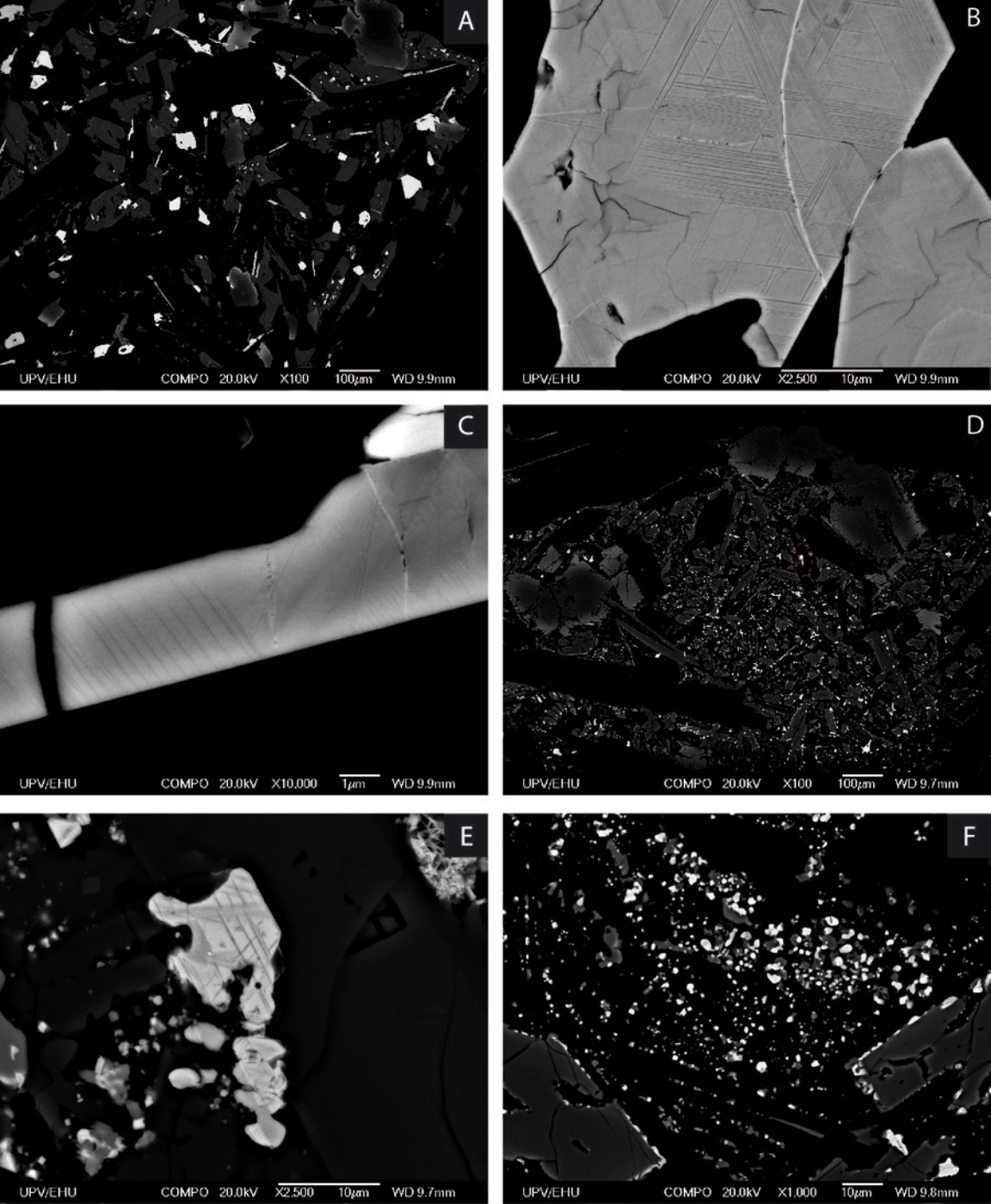
A
UPV/EHU COMPO 20.0kV X100 100µm WD 9.9mm
B
UPV/EHU COMPO 20.0kV X2,500 10µm WD 9.9mm
C
UPV/EHU COMPO 20.0kV X10,000 1µm WD 9.9mm
D
UPV/EHU COMPO 20.0kV X100 100µm WD 9.7mm
E
UPV/EHU COMPO 20.0kV X2,500 10µm WD 9.7mm
F
UPV/EHU COMPO 20.0kV X1,000 10µm WD 9.8mm

Figure 3.

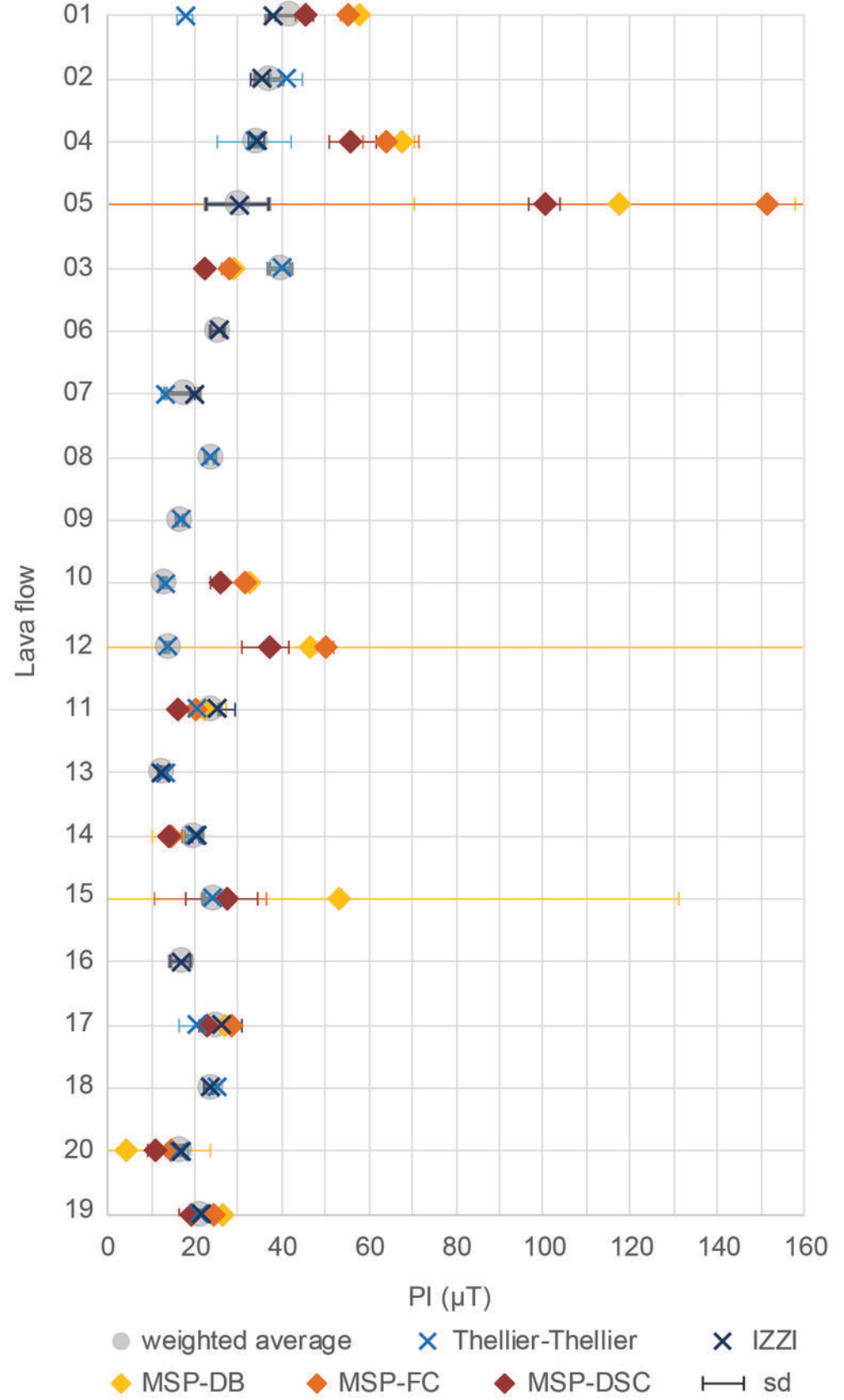
Lava flow
01
02
04
05
03
06
07
08
09
10
12
11
13
14
15
16
17
18
20
19
0
20
40
60
80
100
120
140
160
PI (μT)
weighted average
Thellier-Thellier
IZZI
MSP-DB
MSP-FC
MSP-DSC
sd